Identification and analysis of the signaling pathways, matrix-digestion enzymes, and motility components controlling Vibrio cholerae biofilm dispersal

Andrew Bridges
Princeton University https://orcid.org/0000-0002-8132-751X
Chenyi Fei
Princeton University
Bonnie Bassler (bbassler@princeton.edu)
Princeton Univ. and HHMI https://orcid.org/0000-0002-0043-746X

Article

Keywords: biofilm dispersal, V. cholerae mutants, signal transduction proteins, matrix-degradation enzymes, motility factors

Posted Date: August 25th, 2020

DOI: https://doi.org/10.21203/rs.3.rs-59007/v1

Version of Record: A version of this preprint was published at Proceedings of the National Academy of Sciences on December 7th, 2020. See the published version at https://doi.org/10.1073/pnas.2021166117.

Identification and analysis of the signaling pathways, matrix-digestion enzymes, and motility components controlling *Vibrio cholerae* biofilm dispersal

Andrew A. Bridges[1,2], Chenyi Fei[1], Bonnie L. Bassler[1,2*]

[1]Department of Molecular Biology, Princeton University, Princeton, NJ 08544, USA
[2]The Howard Hughes Medical Institute, Chevy Chase, MD 20815, USA.
*Corresponding author. Email: bbassler@princeton.edu

Abstract (200 words)

Bacteria alternate between being free-swimming and existing as members of sessile multicellular communities called biofilms. The biofilm lifecycle occurs in three stages: cell attachment, biofilm maturation, and biofilm dispersal. *Vibrio cholerae* biofilms are hyper-infectious and biofilm formation and dispersal are considered central to disease transmission. While biofilm formation is well-studied, almost nothing is known about biofilm dispersal. Here, we conduct an imaging screen for *V. cholerae* mutants that fail to disperse, revealing three classes of dispersal components: signal transduction proteins, matrix-degradation enzymes, and motility factors. Signaling proteins dominated the screen and among them, we focused on an uncharacterized two-component sensory system that we name DbfS/DbfR for Dispersal of Biofilm Sensor/Regulator. Phospho-DbfR represses biofilm dispersal. DbfS dephosphorylates and thereby inactivates DbfR, which permits dispersal. Matrix degradation requires two enzymes: LapG, which cleaves adhesins, and RbmB, which digests matrix polysaccharide. Reorientations in swimming direction, mediated by CheY3, are necessary for cells to escape from the porous biofilm matrix. We suggest that these components act sequentially: signaling launches dispersal by terminating matrix production and triggering matrix digestion and, subsequently, cell motility permits escape from biofilms. This study lays the groundwork for interventions that modulate *V. cholerae* biofilm dispersal to ameliorate disease.

Main

Bacteria transition between existing in the biofilm state, in which cells are members of surface-associated multicellular collectives, and living as free-swimming, exploratory individuals. Biofilms consist of cells surrounded by a self-secreted extracellular matrix that protects the resident cells from threats including predation, antimicrobials, and dislocation due to flow.[1–3] Biofilms are relevant to human health because beneficial microbiome bacteria exist in biofilms, and, during disease, because pathogens in biofilms evade host immune defenses, thwart medical intervention, and exhibit virulence.[4–7] The biofilm lifecycle consists of three stages: cell attachment, biofilm maturation, and dispersal (Fig. 1A).[8] Cells liberated during the dispersal step can disseminate and found new biofilms.[8] The environmental stimuli and the components facilitating biofilm attachment and maturation have been defined for many bacterial species.[9] In contrast, little is known about the biofilm dispersal stage.

The model pathogen *Vibrio cholerae* forms biofilms in its aquatic habitat, biofilm cells are especially virulent in mouse models of cholera disease, and biofilms are thought to be critical for cholera transmission.[10–14] Studies of *V. cholerae* biofilms have predominantly focused on matrix overproducing strains that constitutively exist in the biofilm mode and that do not disperse. This research strategy has propelled understanding of *V. cholerae* biofilm attachment and maturation, revealing that the second messenger cyclic diguanylate (c-di-GMP) is a master regulator of biofilm formation, and that expression of vibrio polysaccharide (*vps*) biosynthetic genes are required.[15–17] The strategy of characterizing constitutive biofilm formers, while successful for uncovering factors that promote biofilm formation, has necessarily precluded studies of biofilm dispersal. Here, we employed a microscopy assay that allowed us to monitor the full wild-type (WT) *V. cholerae* biofilm lifecycle. We combined this assay with high-content imaging of randomly mutagenized WT *V. cholerae* to identify genes required for biofilm dispersal. Investigation of the proteins encoded by the genes allowed us to characterize the signaling relays, matrix-digestion enzymes, and motility components required for biofilm dispersal, a key stage in the lifecycle of the global pathogen *V. cholerae.*

Results

Previously, we developed a brightfield microscopy assay that allows us to monitor the full WT *V. cholerae* biofilm lifecycle in real time.[18] In our approach, *V. cholerae* cells are inoculated onto glass coverslips at low cell density and brightfield time-lapse microscopy is used to monitor biofilm progression. WT biofilms reach peak biomass after 8-9 h of incubation and subsequently dispersal occurs and is completed by 12-13 h (Fig. 1B, C). To identify genes required for biofilm dispersal, we combined mutagenesis with high-content imaging of the output of this assay. Specifically, WT *V. cholerae* was mutagenized with Tn*5* yielding ~7000 mutants that were arrayed in 96-well plates. Following overnight growth, the mutants were diluted to low cell density in minimal medium, a condition that drives initiation of the biofilm lifecycle. Brightfield images of each well were captured 8 h post-inoculation to assess biofilm maturation and at 13 h to evaluate biofilm dispersal. Mutants that showed no defects in biofilm maturation as judged by the 8 h images but displayed significant remaining biofilm biomass at the 13 h timepoint were identified. To verify phenotypes, candidate mutants were individually reevaluated by time-lapse microscopy. Mutants that accumulated at the bottom of wells due to aggregation or that failed to attach to surfaces were excluded from further analysis, eliminating strains harboring insertions in O-antigen and flagellar genes, respectively. The locations of transposon insertions in the 47 mutants that met our criteria were defined and corresponded to 10 loci. The new genes from the screen fell into

three classes: signal transduction (blue), matrix degradation (green), and motility (red) (Fig. 1A, C). In-frame deletions of each gene were constructed, and the biofilm lifecycles of the deletion mutants were imaged to confirm that the genes are required for biofilm dispersal (Table 1, Supplementary Video 1). We also identified insertions in genes encoding proteins with known roles in biofilm dispersal (i.e., RpoS, quorum sensing), which we excluded from further analysis.[18,19]

Figure 1

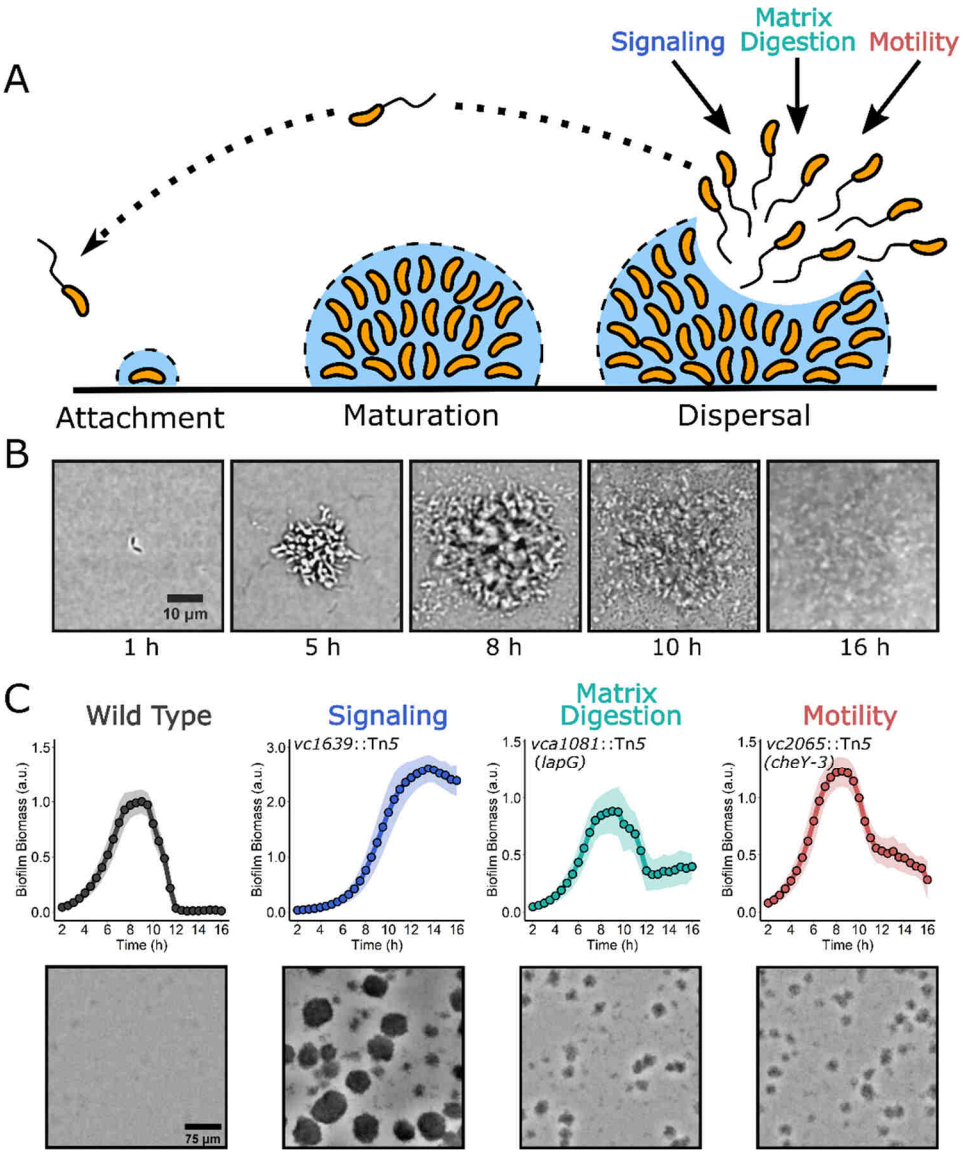

Fig. 1. **A high-content imaging screen identifies genes required for *V. cholerae* biofilm dispersal.** (A) Schematic illustrating the *V. cholerae* biofilm lifecycle. See text for details. (B) Brightfield image series over time of the WT *V. cholerae* biofilm lifecycle. (C) Top panels: Quantitation of biofilm biomass over time as measured by time-lapse microscopy for WT and representative transposon insertion mutants from each of the three functional categories identified in the screen. Note differences in *y*-axes scales. Data are represented as means normalized to the peak biofilm biomass of the WT strain. $N = 3$ biological and $N = 3$ technical replicates, ± SD (shaded). a.u., arbitrary unit. Bottom panels: Representative brightfield images of biofilms at the final 16 h timepoint for the strains presented in the top panels.

Proteins involved in signal transduction dominated the screen (7 of 10 loci) and included the ribosome-associated GTPase, BipA, multiple cyclic diguanylate (c-di-GMP) signaling proteins, polyamine signaling proteins, and a putative two-component histidine kinase, Vc1639. The signal transduction mutants displayed different severities in their biofilm dispersal phenotypes. The Δ*bipA* displayed a modest defect: ~19% of its biofilm biomass remained at 16 h, the final timepoint of our data acquisition, while the WT showed ~6% biomass remaining. By contrast, the Δ*vc1639* mutant underwent no appreciable dispersal (Table 1). In the category of matrix degradation, two enzymes were identified, LapG a periplasmic protease, and RbmB, a putative polysaccharide lyase (Table 1). A single motility mutant was identified with an insertion in the gene encoding the chemotaxis response regulator *cheY3* (Table 1). Below, we carry out mechanistic studies on select mutants from each category to define the functions of the components. Other mutants will be characterized in separate reports.

Table 1: Genes identified as required for *V. cholerae* biofilm dispersal and phenotypes of deletion mutants.

Gene	Function	Times Hit	Peak Biomass (vs WT)	Peak Time	% Biomass Remaining (16 h)
WT	-	-	1.0 ± 0.2	8.7 ± 0.4 h	6 ± 4%
bipA (*vc2744*)	ribosome-associated GTPase	2	1.0 ± 0.2	9.6 ± 0.3 h	19 ± 6%
cdgG (*vc0900*)	GGDEF domain containing protein	1	1.1 ± 0.3	8.4 ± 0.6 h	34 ± 13%
cdgI (*vc0658*)	c-di-GMP phosphodiesterase	1	0.9 ± 0.2	8.7 ± 0.4 h	17 ± 9%
rocS (*vc0653*)	c-di-GMP phosphodiesterase	1	1.3 ± 0.3	10.4 ± 0.6 h	59 ± 13%
mbaA (*vc0703*)	polyamine sensor, c-di-GMP phosphodiesterase	2	0.9 ± 0.2	9.6 ± 0.3 h	27 ± 10%
potD1 (*vc1424*)	polyamine transporter	6*	1.6 ± 0.2	11.9 ± 0.9 h	90 ± 12%
dbfS (*vc1639*)	histidine kinase	8	1.8 ± 0.3	14.3 ± 0.9 h	95 ± 8%
lapG (*vca1081*)	peptidase	3	0.8 ± 0.2	9.4 ± 0.2 h	55 ± 12%
rbmB (*vc0929*)	polysaccharide lyase	21	0.9 ± 0.2	10 ± 0.4 h	69 ± 12%
cheY3 (*vc2065*)	chemotaxis response regulator	2*	1.0 ± 0.2	9.1 ± 0.6 h	21 ± 6%

All ± values represent SD
*Value includes transposon insertions in other genes in this operon

A two-component regulatory system controls *V. cholerae* biofilm dispersal

The mutant from our screen that exhibited the most extreme dispersal phenotype had a transposon in a gene encoding an uncharacterized putative histidine kinase (designated HK), Vc1639 (Table 1). A screen for factors required for *V. cholerae* colonization of the suckling mouse intestine repeatedly identified Vc1639, suggesting that this HK is core to the cholera disease.[20] HKs typically contain periplasmic ligand binding domains and internal catalytic domains that switch between kinase and phosphatase activities based on ligand detection.[21] HKs transmit sensory information to cognate response regulators (RR) by altering RR phosphorylation.[22] RRs, in turn, control gene expression and/or behavior depending on their phosphorylation states. Deletion of *vc1639* in *V. cholerae* resulted in an 80% increase in peak biofilm biomass relative to WT and nearly all the biofilm biomass remained at 16 h demonstrating that Vc1639 is essential for biofilm dispersal (Fig. 2A, Table 1). Complementation of the Δ*vc1639* mutant with *vc1639* inserted onto the chromosome at an ectopic locus restored WT biofilm dispersal (Extended Data Fig. 1A). Consistent with the extreme dispersal phenotype of the Δ*vc1639* mutant, *vpsL-lux* expression was elevated 10-fold throughout the growth curve in the Δ*vc1639* strain compared to WT *V. cholerae* (Fig. 2B). *vpsL* is the first gene in the major extracellular matrix biosynthetic operon showing that Vc1639 signaling regulates matrix production. *vc1639* is the final gene in a three gene operon that includes genes encoding a hypothetical protein (Vc1637) and an OmpR family RR (Vc1638) (Fig. 2C). We name Vc1639 DbfS for Dispersal of Biofilm Sensor and we name Vc1638 DbfR for Dispersal of Biofilm Regulator. Domain prediction suggests that DbfS contains two transmembrane domains (TM), a periplasmic sensory domain, and a cytoplasmic HAMP domain that likely transmits ligand-binding-induced conformational changes to regulation of the C-terminal kinase/phosphatase activity (Fig. 2C).

To explore the connection between DbfS and DbfR in the control of biofilm dispersal, we deleted *dbfR*. Typically, cognate HK and RR null mutants have identical phenotypes. To our surprise, the Δ*dbfR* mutant had no biofilm dispersal defect and progressed through the biofilm lifecycle identically to WT (Fig. 2D). We considered the possibility that some other RR is the partner to DbfS. To test this idea, we constructed the Δ*dbfS* Δ*dbfR* double mutant. This strain behaved identically to the Δ*dbfR* strain (Fig. 2D), demonstrating that *dbfR* is epistatic to *dbfS* and thus, DbfR indeed functions downstream of DbfS. Moreover, because RRs are typically active when phosphorylated, our results suggest that DbfR must be active in the absence of DbfS. Thus, we reason that phospho-DbfR is the species present in the Δ*dbfS* strain. To verify the hypothesis that phospho-DbfR is responsible for the dispersal defect in the Δ*dbfS* strain, we constructed a non-phosphorylatable allele of DbfR (D51V). The *V. cholerae* $dbfR^{D51V}$ mutant displayed the WT biofilm dispersal phenotype in the presence and the absence of DbfS (Fig. 2E). DbfR-SNAP fusions showed that SNAP did not interfere with WT DbfR function and that DbfR protein abundance was unchanged in the $dbfR^{D51V}$ strain relative to WT (Extended Data Fig. 1B, C). Thus, phospho-DbfR causes *V. cholerae* cells to remain in the biofilm state in the Δ*dbfS* mutant. It follows that deletion of *dbfS* causes biofilm dispersal failure due to loss of DbfS phosphatase activity on DbfR. To test this hypothesis, we assessed *in vivo* DbfR phosphorylation in the presence and absence of DbfS. Phos-tag gel analysis enabled separation and visualization of phosphorylated and dephosphorylated DbfR. In the absence of DbfS, DbfR was phosphorylated and induction of DbfS production caused the phospho-DbfR species to disappear (Fig. 2F). Thus, under our experimental conditions, DbfS functions as a DbfR phosphatase. We infer that some other unknown kinase must exist and phosphorylate DbfR (Fig. 2G). We propose that phospho-DbfR is active, and it drives expression of matrix biosynthetic genes, and increased

Figure 2

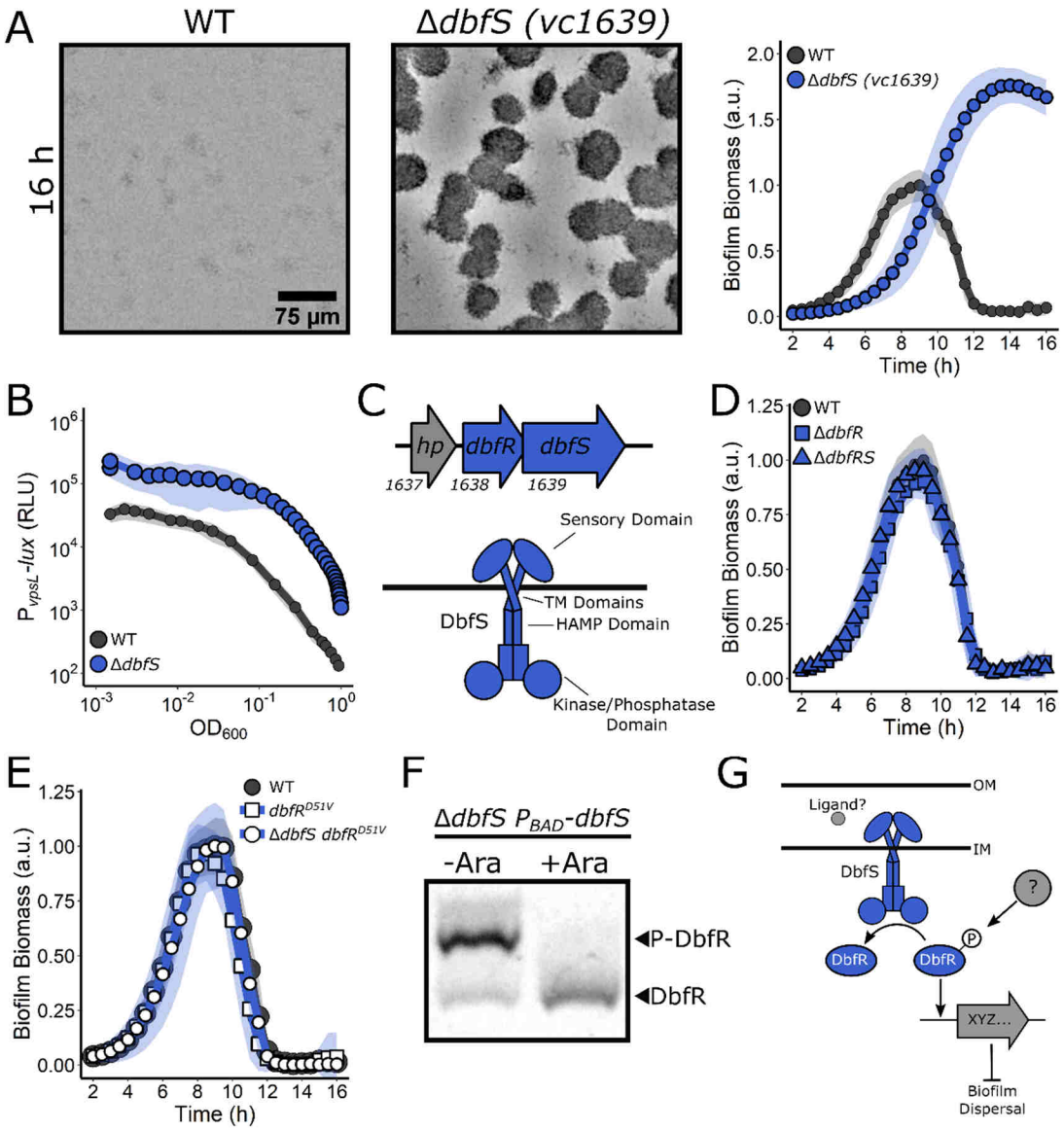

Fig. 2. **A two-component system that we name DbfS (HK) and DbfR (RR) regulates *V. cholerae* biofilm dispersal.** (A) Representative 16 h images and quantitation of biofilm biomass over time measured by time-lapse microscopy for WT *V. cholerae* and the Δ*dbfS* (i.e., Δ*vc1639*) mutant. (B) The corresponding P_{vpsL}-*lux* output for strains and growth conditions in A over the growth curve. (C) Top panel: operon structure of the genes encoding the DbfS-DbfR two-component system. Bottom panel: Cartoon of the domain organization of DbfS. TM, transmembrane domain (D) As in A for the Δ*dbfR* (i.e., Δ*vc1638*) strain and for the Δ*dbfS* Δ*dbfR* double mutant. (E) As in A for the $dbfR^{D51V}$ and Δ*dbfS* $dbfR^{D51V}$ strains. (F) Representative Phos-tag gel analysis of DbfR-SNAP in the absence (-arabinose) or presence (+arabinose) of DbfS. Fucose was added to repress DbfR production in the uninduced samples. A phosphorylated protein migrates slower than the same unphosphorylated protein. (G) Proposed model for the DbfS-DbfR phosphorylation cascade regulating biofilm dispersal. OM, outer membrane; IM, inner membrane. In all biofilm measurements, N = 3 biological and N = 3 technical replicates, ± SD (shaded). a.u., arbitrary unit. For *vpsL-lux* measurements, N = 3 biological replicates, ± SD (shaded). RLU, relative light units. Phos-tag gel result is representative of N = 3 biological replicates.

matrix production prevents biofilm dispersal. It is possible that phospho-DbfR also controls other genes involved in suppressing biofilm dispersal.

BLAST analysis of the DbfS protein sequence against the *Escherichia coli* K-12 genome revealed limited homology to the cation regulated HK, PhoQ, with 32% sequence identity (E value=$1e^{-41}$), with the lowest region of similarity in the predicted ligand binding domain. We tested whether the ligands that control PhoQ signal transduction also regulate DbfS-DbfR signaling (Extended Data Fig. 2A-D, Supplemental Discussion). They do not. Thus, DbfS and DbfR are not functionally equivalent to PhoQ and its cognate RR, PhoP, respectively. Thus, DbfS responds to a yet-to-be defined stimulus to regulate biofilm dispersal.

Matrix disassembly mediates *V. cholerae* exit from biofilms

The second group of mutants in our screen harbored insertions in the gene encoding the calcium-dependent periplasmic protease LapG that degrades outer-membrane spanning adhesive proteins and in the gene specifying the extracellular polysaccharide lyase RbmB that degrades the VPS component of the biofilm matrix.[23,24] The Δ*lapG* strain exhibited slightly lower peak biofilm biomass compared to WT, with a short delay in the onset of dispersal, and ~55% of its biomass remained at 16 h (Fig. 3A, Table 1). The Δ*lapG* and the WT strains had similar *vpsL-lux* expression patterns (Fig. 3B) consistent with LapG playing no role in repression of matrix production, but rather functioning downstream in matrix degradation. The LapG mechanism is known: When c-di-GMP concentrations are high, the FrhA and CraA adhesins are localized to the outer membrane where they facilitate attachments that are important for biofilm formation (Fig. 3C).[25,26] Under this condition, LapG is sequestered and inactivated by the inner membrane c-di-GMP sensing protein LapD.[25] When c-di-GMP levels fall, LapD releases LapG, and LapG cleaves FrhA and CraA facilitating cell detachment from biofilms.[25] Our results are consistent with this mechanism; in the absence of LapG, FrhA and CraA remain intact, and *V. cholerae* cells cannot properly exit the biofilm state. To verify that the established c-di-GMP-dependent regulatory mechanism controls LapG activity in our assay, we deleted *lapD* (Fig. 3C). Indeed, in the Δ*lapD* strain, biofilm dispersal occurred prematurely indicating that, without LapD, LapG is not sequestered, and unchecked LapG activity promotes premature adhesin degradation, and, as a consequence, early biofilm disassembly (Fig. 3D). The Δ*lapD* Δ*lapG* double mutant had the same dispersal phenotype as the Δ*lapG* single mutant confirming that LapG functions downstream of LapD (Fig. 3D). Lastly, in a reciprocal arrangement, overexpression of *lapG* from an ectopic locus caused peak biofilm formation to decrease by ~65% (Extended Data Fig. 3A) suggesting that enhanced LapG-mediated cleavage of adhesins prematurely released cells from the biofilm. Thus, the conserved Lap pathway, which responds to changes in c-di-GMP levels, facilitates biofilm dispersal in *V. cholerae*.

Regarding the RbmB polysaccharide lyase, the Δ*rbmB* strain formed biofilms to roughly the same peak biomass as WT, however, it exhibited a 2 h delay in dispersal onset and most of its biomass (~70%) remained at 16 h (Fig. 3E, Table 1). The level of *vpsL-lux* expression in the Δ*rbmB* mutant was similar to the WT, showing that the RbmB dispersal function does not concern production of VPS (Fig. 3F). Complementation with inducible *rbmB* expressed from an ectopic locus in the Δ*rbmB* strain caused a ~40% reduction in peak biofilm formation, confirming that RbmB negatively regulates biofilm formation, however the complemented strain retained a modest biofilm dispersal defect, suggesting that the timing or level of *rbmB* expression is critical for WT biofilm disassembly (Extended Data Fig. 3B). To verify that the Δ*rbmB* dispersal defect stems from the lack of *vps* degradation, we grew Δ*rbmB* biofilms for 16 h (i.e., post WT biofilm

Figure 3

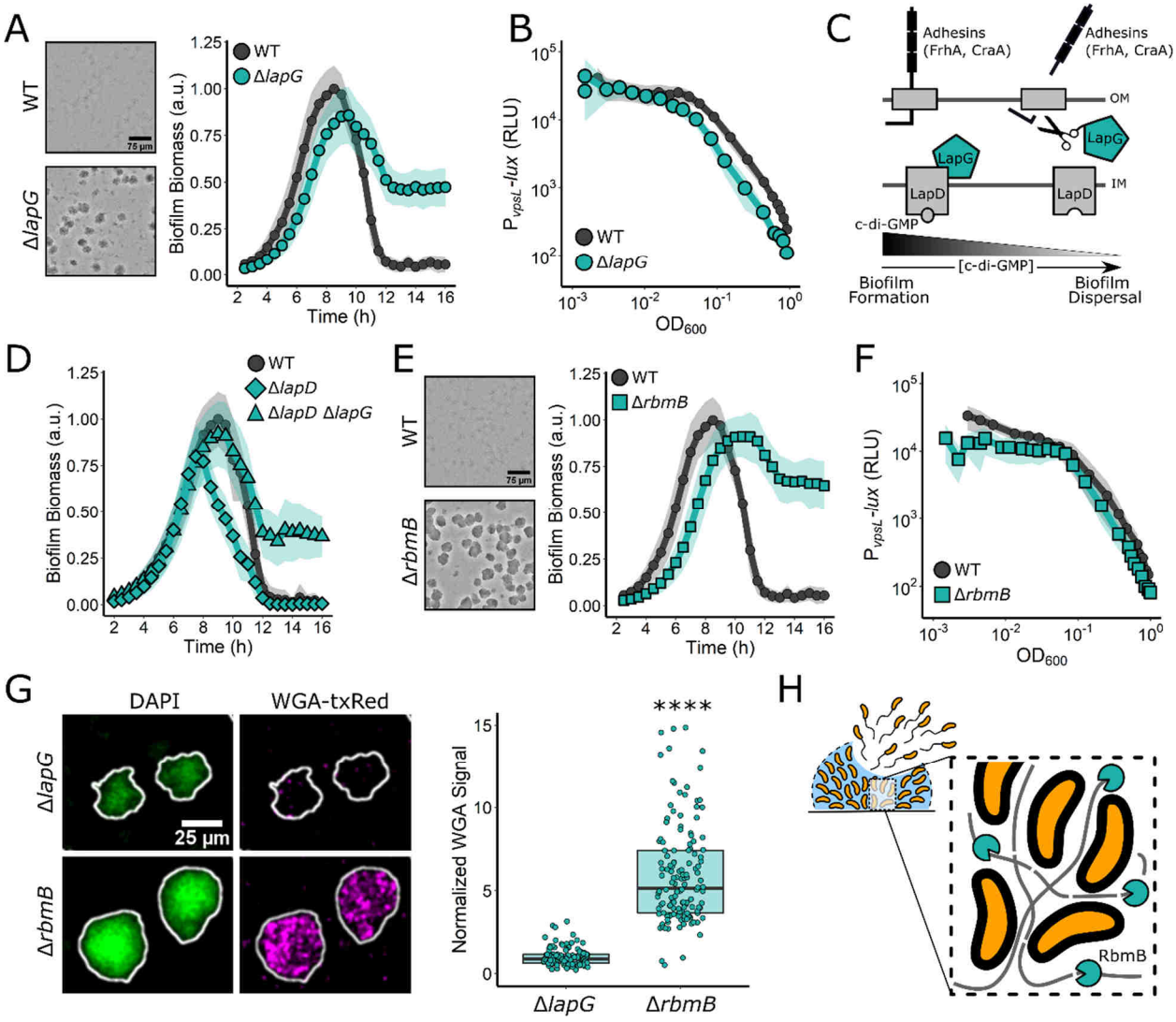

Fig. 3. **Matrix-digesting enzymes mediate *V. cholerae* biofilm dispersal.** (A) Representative 16 h images and quantitation of biofilm biomass over time measured by time-lapse microscopy for WT *V. cholerae* and the Δ*lapG* mutant. (B) The corresponding P_{vpsL}-*lux* output for strains and growth conditions in A over the growth curve. (C) Schematic representing the LapG mechanism. (D) As in A for the WT, the Δ*lapD* single mutant, and the Δ*lapD* Δ*lapG* double mutant. (E) As in A for the WT and the Δ*rbmB* mutant. (F) As in B for WT *V. cholerae* and the Δ*rbmB* mutant. (G) Representative images and quantitation of WGA-txRed signal in Δ*lapG* and Δ*rbmB* biofilms 16 h post-inoculation. To account for differences in biomass, the WGA-txRed signal was divided by the 4', 6-diamidino-2-phenylindole (DAPI) signal in each biofilm. Values were normalized to the mean signal for the Δ*lapG* strain. >100 individual biofilms were quantified for each strain. An unpaired t-test was performed for statistical analysis, with **** denoting $p < 0.0001$. (H) Proposed model for the role of RbmB in biofilm dispersal. Gray lines represent the polysaccharide matrix. In all cases, $N = 3$ biological and $N = 3$ technical replicates, ± SD (shaded). a.u., arbitrary unit. For *vpsL-lux* measurements, $N = 3$ biological replicates, ± SD (shaded). RLU, relative light units. OM, outer membrane; IM, inner membrane.

dispersal completion), and subsequently fixed and stained the non-dispersed biofilms with wheat germ agglutinin conjugated to Texas Red (WGA-txRed), which binds to N-acetylglucosamine sugars in the VPS matrix.[27] We used the Δ*lapG* mutant as our control since its biofilm dispersal phenotype should not involve changes in VPS. On average, the Δ*rbmB* mutant exhibited ~6x more WGA-txRed signal than the Δ*lapG* mutant (Fig. 3G). Collectively, our results show that the non-dispersed Δ*lapG* biofilms contain little VPS, consistent with possession of functional RbmB, while non-dispersed Δ*rbmB* biofilms contain excess VPS due to the lack of RbmB-mediated polysaccharide digestion. Thus, we suggest that RbmB-directed VPS disassembly is critical for proper biofilm disassembly (Fig. 3H).

Extracellular DNA (eDNA) is a component of the *V. cholerae* biofilm matrix and two DNAses secreted by *V. cholerae*, Dns and Xds, digest eDNA.[28] Although we did not identify *dns* and *xds* in our screen, we nonetheless investigated whether they contributed to biofilm dispersal. Neither the Δ*dns* and the Δ*xds* single mutants, nor the Δ*dns* Δ*xds* double mutant displayed a biofilm dispersal defect in our assay (Extended Data Fig. 3C), suggesting that eDNA digestion is not required for dispersal. In a similar vein, we did not identify genes encoding the eight *V. cholerae* extracellular proteases that could degrade matrix proteins. Consistent with this finding, measurement of the phenotypes of mutants deleted for each extracellular protease gene showed that none exhibited a dispersal defect. Thus, no single extracellular protease is required for biofilm dispersal (Extended Data Fig. 3D). It remains possible that proteases contribute to biofilm dispersal by functioning redundantly. Together, our results indicate that two enzymes, LapG and RbmB, are the primary matrix degrading components that enable biofilm dispersal.

Reorientations in swimming direction are required for biofilm dispersal.

The final category of genes identified in our screen are involved in cell motility. As noted above, non-motile mutants were excluded from analysis because they are known to be impaired in surface attachment. Nonetheless, we identified a mutant containing a transposon insertion in *cheY3* as defective for biofilm dispersal. *cheY3* is one of the five *V. cholerae cheY* genes specifying chemotaxis RR proteins.[29] Notably, *cheY3* is the only *V. cholerae cheY* homolog required for chemotaxis.[29] The Δ*cheY3* mutant exhibited similar peak biofilm timing and biomass as WT *V. cholerae*, however, ~21% biomass remained at 16 h (Fig. 4A, Table 1). Expression of *vpsL-lux* in the mutant was identical to the WT indicating that the dispersal phenotype was not due to elevated matrix production (Fig. 4B).

The *V. cholerae* default motor rotation direction is counterclockwise (CCW), which fosters smooth, straight swimming.[30] Transition to clockwise (CW) motor rotation causes reorientations in swimming direction.[30] Phospho-CheY3 binds to the flagellar motor switch complex to mediate the change from CCW to CW rotation. Thus, the Δ*cheY3* mutant is non-chemotactic and the cells are locked in the CCW, straight swimming mode (Fig. 4C). We reasoned that the Δ*cheY3* mutant dispersal defect could stem from an inability to chemotact or from an inability to reorient swimming direction. To distinguish between these possibilities, we examined biofilm dispersal in a *V. cholerae* mutant carrying a *cheY3* allele, $cheY3^{D16K,\ Y109W}$ (henceforth, *cheY3**) that locks the motor into CW rotation and so also disrupts chemotaxis. *cheY3** cells undergo frequent reorientations and are unable to swim in smooth straight runs (Fig. 4C).[29,31] The *cheY3** strain had WT biofilm dispersal capability. Thus, being chemotactic is not required for *V. cholerae* to exit biofilms (Fig. 4A).

We reasoned that analysis of the unique motility characteristics of our strains could reveal

the underlying causes of the Δ*cheY3* biofilm dispersal defect. We measured the turning frequencies and swimming velocities of the WT, Δ*cheY3*, and *cheY3* V. cholerae* strains. Consistent with previous reports, these three mutants exhibited notable differences: on average, the WT turned once every 3 s, the Δ*cheY3* mutant turned less than once every 40 s, and the *cheY3** strain turned once every 0.5 s (Fig. 4C and D).[29,31] The *cheY3** strain displayed slightly lower average swimming velocity than the WT and Δ*cheY3* strains, due to its high turning frequency as turning necessarily involves a decrease in velocity (Fig. 4E).[32] Together, these results suggest that the low turning frequency of the Δ*cheY3* mutant is responsible for the biofilm dispersal defect. We propose that if cells do not frequently change their direction of motion, they become trapped by the biofilm matrix mesh which compromises their ability to escape (Fig. 4F). Indeed, in other bacteria, straight-swimming mutants are deficient in traversing fluid-filled porous media compared to WT organisms that can reorient.[33] Together, these results indicate that chemotaxis itself is not required for biofilm dispersal, but, rather, that the chemotaxis machinery facilitates random reorientation events that allow *V. cholerae* cells to navigate a porous biofilm matrix. The same non-chemotactic mutants used here exhibit stark differences in competition experiments in animal models of cholera infection, showing that their differences in motility and, possibly, their differences in biofilm dispersal capabilities, are pertinent to colonization.[31]

Finally, we determined whether the ability to locomote was required for biofilm dispersal or, by contrast, if non-motile cells could escape the digested matrix via Brownian motion. As mentioned above, we could not simply study dispersal of non-flagellated and non-motile mutants because of their confounding surface attachment defects and feedback on biofilm regulatory components.[34,35] To circumvent this problem, we employed phenamil, an inhibitor of the Na^+-driven *V. cholerae* flagellar motor, which, as expected, dramatically reduced planktonic cell motility (Extended Data Fig. 4).[36] To assess the role of swimming motility in biofilm dispersal, we first allowed WT *V. cholerae* cells to undergo biofilm formation for 5 h, at which point we perfused DMSO or phenamil into the incubation chamber (Fig. 4G). Following phenamil treatment, the WT strain displayed a dispersal defect nearly identical to that of the Δ*cheY3* mutant. Additionally, phenamil treatment of the Δ*cheY3* mutant did not further impair its biofilm dispersal. Together, these results demonstrate that swimming motility is crucial for *V. cholerae* biofilm dispersal and an inability to reorient is as detrimental to dispersal as a complete lack of flagellar motility.

Discussion

In this study, we developed a high-content imaging screen that allowed us to identify components required for *V. cholerae* biofilm dispersal. We categorized the identified components into three classes: signal transduction, matrix disassembly, and cell motility. We propose that the three functional categories represent the chronological steps required for the disassembly of a biofilm: First, the stimuli that activate dispersal must accumulate. Subsequently, the gene expression pattern established by detection of these stimuli must repress biofilm matrix production and activate production of enzymes required to digest the biofilm matrix. Finally, cells must escape through the partially digested, porous matrix which requires changes in the direction of movement. Together, these steps ensure that when environmental conditions are appropriate, *V. cholerae* cells can exit the sessile lifestyle and disseminate to new terrain that is ripe for biofilm formation or, alternatively, during disease, to a new host. One can now imagine targeting the functions identified in this work for small-molecule disruption of the *V. cholerae* biofilm lifecycle, possibly guiding the development of treatments to reduce the duration of *V. cholerae* infection or to prevent transmission.

Figure 4

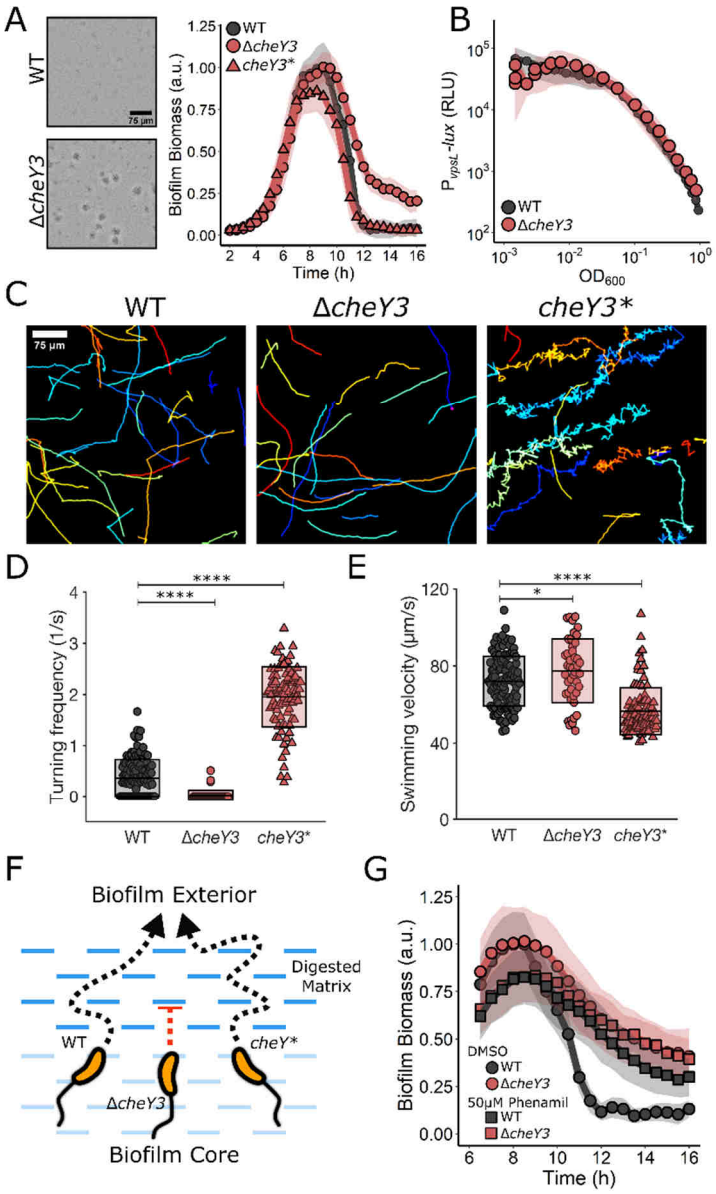

Fig. 4. **Reorientations in swimming direction are required for *V. cholerae* biofilm dispersal.** (A) Representative 16 h images and quantitation of biofilm biomass over time measured by time-lapse microscopy for WT *V. cholerae*, the Δ*cheY3* mutant, and the *cheY3*$^{D16K, Y109W}$ (*cheY3**) mutant. (B) The corresponding P_{vpsL}-*lux* output for WT and the Δ*cheY3* strain over the growth curve. (C) Representative, randomly colored, single-cell locomotion trajectories for the strains in A. (D) Turning frequencies of the strains in A. (E) Measured swimming velocities of the strains in A. (F) Proposed model for the role of motility and reorientation in biofilm dispersal. (G) Quantitation of biofilm biomass over time for WT and the Δ*cheY3* mutant following treatment with DMSO or the motility inhibitor, phenamil supplied at 5 h post-inoculation. For biofilm biomass assays, $N = 3$ biological and $N = 3$ technical replicates, ± SD (shaded). a.u., arbitrary unit. For *vpsL-lux* measurements, $N = 3$ biological replicates, ± SD (shaded). RLU, relative light units. For motility measurements, 45-125 individual cells of each strain were tracked. In panels D and E, unpaired t-tests were performed for statistical analysis, with P values denoted as *P < 0.05; **P < 0.01; *** P < 0.001; ****P < 0.0001; n.s., P > 0.05.

Materials and Methods

Bacterial Strains and Reagents

The *V. cholerae* parent strain used in this study was WT O1 El Tor biotype C6706str2. Antibiotics were used at the following concentrations: polymyxin B, 50 µg/mL; kanamycin, 50 µg/mL; spectinomycin, 200 µg/mL; and chloramphenicol, 1 µg/mL. Strains were propagated in lysogeny broth (LB) supplemented with 1.5% agar or in liquid LB with shaking at 30°C. All strains used in this work are reported in Supplementary Table 1. Unless otherwise stated, exogenous compounds were added from the onset of biofilm initiation. The antimicrobial peptide C18G (VWR) was added at 5 µg/mL. Phenamil (Sigma) was prepared in DMSO and added 5 h post biofilm inoculation to a final concentration of 50 µM. L-arabinose (Sigma) was prepared in water and added at 0.2%.

DNA Manipulation and Strain Construction

To produce linear DNA fragments for natural transformations, splicing overlap extension PCR was performed using iProof polymerase (Bio-Rad, Hercules, CA, USA) to combine DNA pieces. Primers and gene fragments used in this study are reported in Supplementary Table 2. In all cases, ~3 kb of upstream and downstream flanking regions of homology were generated by PCR from *V. cholerae* genomic DNA and were included to ensure high chromosomal integration frequency. DNA fragments that were not native to *V. cholerae* were synthesized as g-blocks (IDT, Coralville, IA, USA).

All *V. cholerae* strains generated in this work were constructed by replacing genomic DNA with DNA introduced by natural transformation as previously described.[18,37] PCR and Sanger sequencing were used to verify correct integration events. Genomic DNA from recombinant strains was used for future co-transformations and as templates for PCR to generate DNA fragments, when necessary. Deletions were constructed in frame and eliminated the entire coding sequences. The exceptions were *mbaA*, *dbfS*, and *dbfR*, which each overlap with another gene in their operons. In these cases, portions of the genes were deleted ensuring that adjacent genes were not perturbed. For *tagA*, the first 103 base pairs, including the nucleotides specifying the start codon, were deleted. All strains constructed in this study were verified by sequencing at Genewiz.

Microscopy and Mutant Screening

The biofilm lifecycle was measured using time-lapse microscopy as described previously.[18] All plots were generated using ggplot2 in R. To generate the library of *V. cholerae* insertion mutants for the dispersal screen, the WT parent strain was mutagenized with Tn*5* as previously described. Mutants were selected by growth overnight on LB plates containing polymyxin B and kanamycin. The next day, mutant colonies were arrayed into 96-well plates containing 200 µL of LB medium supplemented with polymyxin B and kanamycin using an automated colony-picking robot (Molecular Devices). The arrayed cultures were grown in a plate-shaking incubator at 30° C covered with breathe-easy membranes to minimize evaporation. After 16 h of growth, the arrayed cultures were diluted 1:200,000 into 96-well plates containing M9 medium supplemented with glucose and casamino acids. Diluted cultures were incubated statically at 30° C for 8 h (to achieve peak biofilm biomass), at which point, images of each well were captured on a Nikon Ti-E inverted microscope using transmitted-light bright-field illumination,

a 10× Plan Fluor (NA 0.3) objective lens, and an Andor iXon 897 EMCCD camera. Automated image acquisition was performed using NIS-Elements software v5.11.02 and the NIS-Elements Jobs Module to acquire images at four positions within each well to account for heterogeneity within samples. To maintain the focal plane between wells, the Nikon Perfect Focus System was used. After performing microscopy at the 8 h timepoint, 96-well plates were returned to the incubator. To assess biofilm dispersal, a second set of images of the same samples was acquired at 13 h post inoculation. Mutants that displayed biofilm growth at the 8 h timepoint but failed to disperse by the 13 h timepoint were subcultured, grown overnight, and subsequently re-imaged using the time-lapse approach described above to assess their biofilm lifecycles in real-time. Mutants that exhibited biofilm dispersal defects after this reassessment step were analyzed for the locations of transposon insertions using arbitrary PCR.

vpsL-lux Transcription Assay

Three colonies of each strain to be analyzed were individually grown overnight in 200 µL LB with shaking at 30°C in a 96-well plate covered with a breathe-easy membrane. The following morning, the cultures were diluted 1:5,000 into fresh M9 medium supplemented with glucose and casamino acids. The plates were placed in a BioTek Synergy Neo2 Multi-Mode reader (BioTek, Winooski, VT, USA) under static growth conditions at 30°C. Both OD_{600} and bioluminescence from *vpsL-lux* were simultaneously measured at 15 min time intervals. Results were exported to R, and light values were divided by OD_{600} to produce relative light units (RLUs). Results from replicates were averaged and plotted using ggplot2 in R.

VPS Quantitation

To assess VPS levels in non-dispersed biofilms using WGA-txRED, biofilms were grown for 16 h and subsequently washed 3 times with 1× phosphate buffered saline (PBS), and fixed for 10 min with 3.7% formaldehyde in 1× PBS. After fixation, samples were washed 5 times with 1× PBS and subsequently incubated with a solution containing 1 µg/mL WGA-txRED (ThermoFisher Scientific), 1 µg/mL 4', 6-diamidino-2-phenylindole (DAPI), and 1% bovine serum albumin in 1× PBS for 1 h with shaking at 30° C in the dark. After incubation, samples were washed 5 more times with 1× PBS before imaging. Confocal microscopy was performed on a Leica DMI8 SP-8 point scanning confocal microscope (Leica, Wetzlar, Germany) with the pinhole set to 1.0 airy unit. The light source for DAPI was a 405 laser and the light source used to excite WGA-txRED was a tunable white-light laser (Leica; model #WLL2; excitation window = 470–670 nm) set to 595 nm. Biofilms were imaged using a 10× air objective (Leica, HC PL FLUOTAR; NA: 0.30). Sequential frame scanning was performed to minimize spectral bleed-through in images. Emitted light was detected using GaAsP spectral detectors (Leica, HyD SP), and timed gate detection was employed to minimize the background signal. Image analyses were performed in FIJI software (Version 1.52p). Biofilms were segmented in the DAPI channel using an intensity threshold and the intensities of each channel were measured. The same threshold was applied to all images. WGA-txRED signal was divided by DAPI signal to achieve the normalized WGA signal.

Motility Assay

To prevent biofilm formation during measurements of swimming velocities and turning frequencies for the WT, Δ*cheY3*, and *cheY3** strains, *vpsL* was deleted. Each strain was grown

for 16 h in LB medium and the following day, cells were diluted to OD_{600} = 0.001 in M9 medium supplemented with glucose and casamino acids. Subsequently, diluted cultures were dispensed in 200 µL aliquots into glass-coverslip bottomed 96-well plates (MatTek, Ashland, MA, USA). After a period of 1 h, during which time cells were allowed to adhere to the coverslips, wells were washed 8 times with fresh medium to remove unattached cells. The plates were incubated at 25° C for 3 h, and imaging was performed using the brightfield setup described above for the biofilm dispersal screen. In this case, the frame interval was 50 msec and imaging was conducted at a distance of ~100 µm into the sample. Images were smoothed, background corrected, and imported into the TrackMate (v.5.2.0) plugin in FIJI. Cells were detected with a Laplacian of Gaussian (LoG) detector and were subsequently tracked using the simple Linear Assignment Problem (LAP) approach. To exclude non-motile cells from our analyses in Fig. 4C-E objects with velocities under 40 µm/sec were eliminated. Analyses and plotting of swimming velocities and turning frequencies were performed in MATLAB (The Mathworks, Inc.). Local curvatures for single-cell locomotion trajectories were calculated as described.[38] Curvature of less than 0.3 μm^{-1} was used to identify the turning events. MSD was calculated as described previously.[39]

Phos-tag Gel Analysis

To monitor DbfR and phospho-DbfR via SDS-PAGE, the endogenous *dfbR* gene was replaced with *dbfR-SNAP* in the Δ*dbfS* strain, and P_{BAD}-*dbfS* was introduced at the ectopic locus, *vc1807*. To assess DbfR-SNAP phosphorylation in the absence and presence of DbfS, overnight cultures of the strain were diluted 1:1000 and subsequently grown for 4 h at 30° C with shaking to an OD_{600} ~ 0.6. To each culture, 1 µM SNAP-Cell TMR Star (New England Biolabs) was added to label the SNAP tag, and the culture was subsequently divided into two tubes. To one tube, 0.2% D-fucose was added, and to the other, 0.2% L-arabinose was added to repress and induce DbfS production, respectively. The cultures were returned to 30° C with shaking. After 1 h, the cells were collected by centrifugation for 1 min at 13,000 rpm. Lysis and solubilization were carried out as rapidly as possible. Briefly, cells were chemically lysed by resuspension to OD_{600} = 1.0 in 40 µL Bug Buster (Novagen) for 5 min at 25° C with intermittent vortex. The cell lysate was solubilized at 25° C in 1.5× SDS-PAGE buffer for 5 min also with intermittent vortex. Samples were immediately loaded onto a cold 7.5% SuperSep™ Phos-tag™ (50 µM/L) gel (FUJIFILM Wako Pure Chemical, 198-17981). Electrophoresis was carried out at 100 V at 4° C until the loading buffer exited the gel. Gel images were captured on an ImageQuant LAS 4000 imager (GE Healthcare) using a Cy3 filter set.

Extended Data Fig. 1

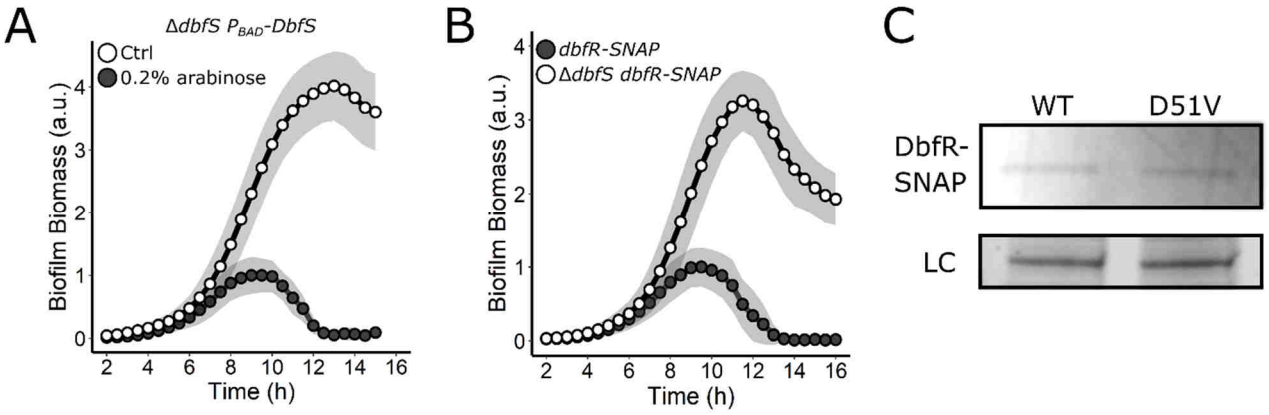

Extended Data Fig. 1. **Complementation, functional tagging, and mutagenesis of the DbfS-DbfR two-component system.** (A) Quantitation of biofilm biomass over time measured by time-lapse microscopy for the Δ*dbfS* P_{BAD}-*dbfS* strain following addition of water (Ctrl) or 0.2% arabinose. (B) As in A for SNAP-tagged DbfR in the WT and Δ*dbfS* strains. (C) Top panel: representative in-gel SDS-PAGE fluorescence following electrophoresis of *V. cholerae* cell lysates containing WT DbfS-SNAP or $DbfS^{D51V}$-SNAP that had been incubated with SNAP-Cell TMR Star. Bottom panel: Coomassie stained loading control (LC). For all biofilm measurements, $N = 3$ biological and $N = 3$ technical replicates, ± SD (shaded). a.u., arbitrary unit.

Extended Data Fig. 2

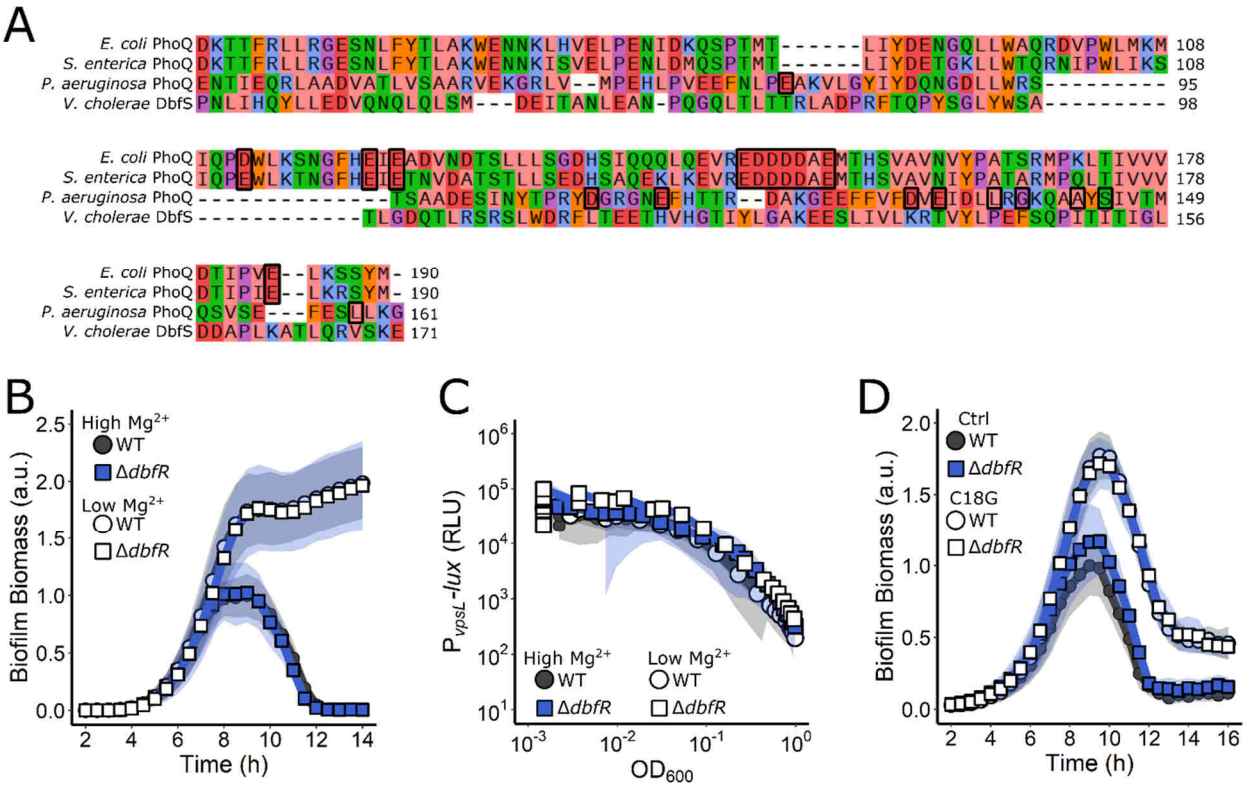

Extended Data Fig. 2. **DbfS is not functionally equivalent to PhoQ.** (A) Alignment of the sensory domains of PhoQ from *E. coli*, *S. enterica*, and *P. aeruginosa* against that of *V. cholerae* DbfS. Black boxes indicate residues involved in Mg^{2+} binding in PhoQ. (B) Quantitation of biofilm biomass over time measured by time-lapse microscopy in high magnesium (10 mM) and limiting magnesium (10 µM) conditions for WT *V. cholerae* and the Δ*dbfR* strain. (C) The corresponding P_{vpsL}-*lux* outputs for strains and growth conditions in B over the growth curve. (D) As in B except following the addition of water or 5 µg/mL C18G. In all cases, $N = 3$ biological and $N = 3$ technical replicates, ± SD (shaded). a.u., arbitrary unit. For *vpsL-lux* measurements, $N = 3$ biological replicates, ± SD (shaded). RLU, relative light units.

Extended Data Fig. 3

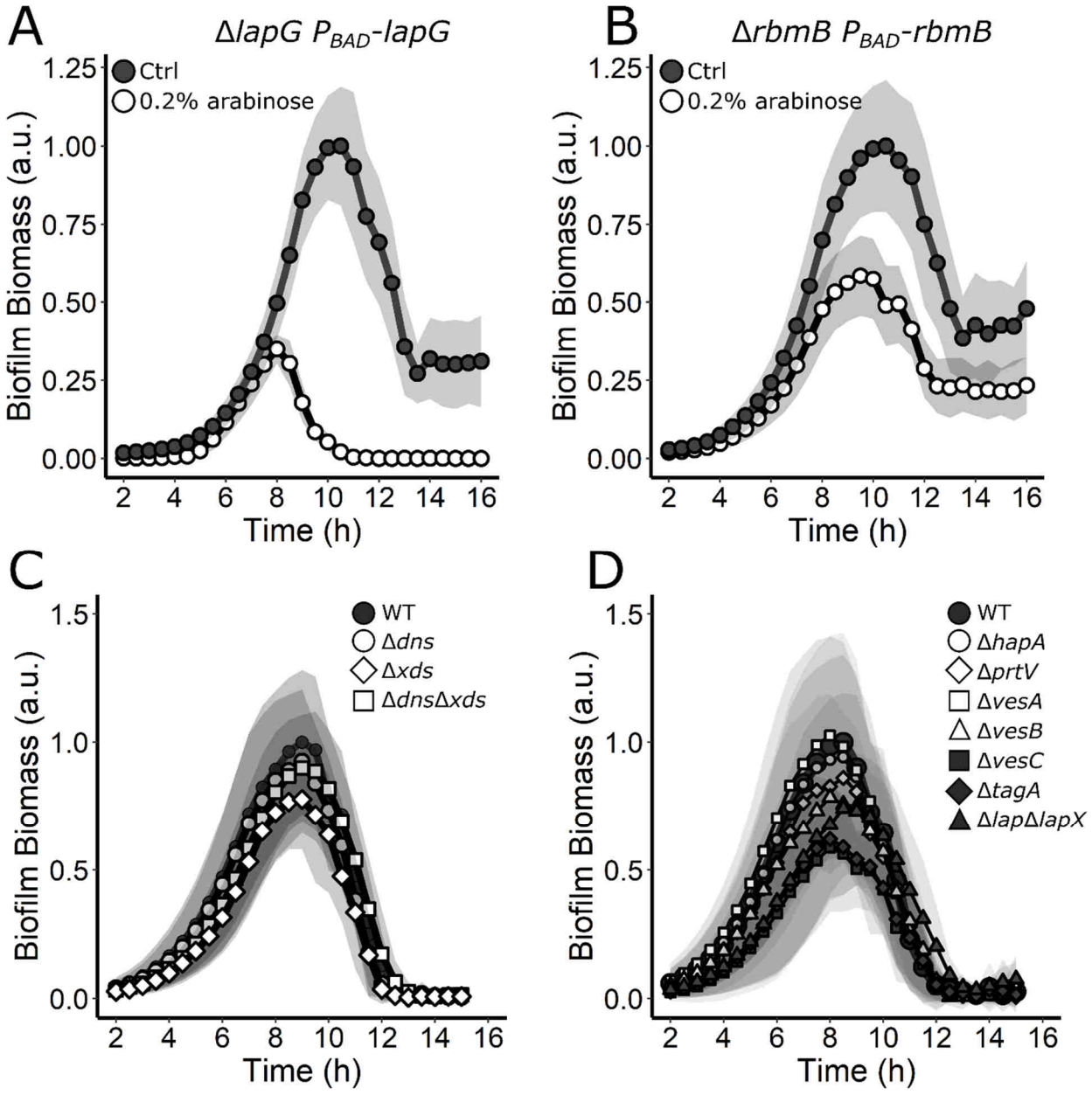

Extended Data Fig. 3. **Introduction of *lapG* and *rbmB* complements the Δ*lapG* and Δ*rbmB* biofilm defects, respectively, and assessment of the roles of extracellular DNAses and secreted proteases in *V. cholerae* biofilm dispersal.** (A) Quantitation of biofilm biomass over time measured by time-lapse microscopy for the Δ*lapG* P_{BAD}-*lapG* strain following addition of water (Ctrl) or 0.2% arabinose. (B) As in A, but for the Δ*rbmB* P_{BAD}-*rbmB* strain. (C) Quantitation of biofilm biomass over time measured by time-lapse microscopy for WT *V. cholerae* and mutants lacking the designated DNAses. (D) Quantitation of biofilm biomass over time measured by time-lapse microscopy for WT *V. cholerae* and mutants lacking the designated proteases. In all cases, $N = 3$ biological and $N = 3$ technical replicates, ± SD (shaded). a.u., arbitrary unit.

Extended Data Fig. 4

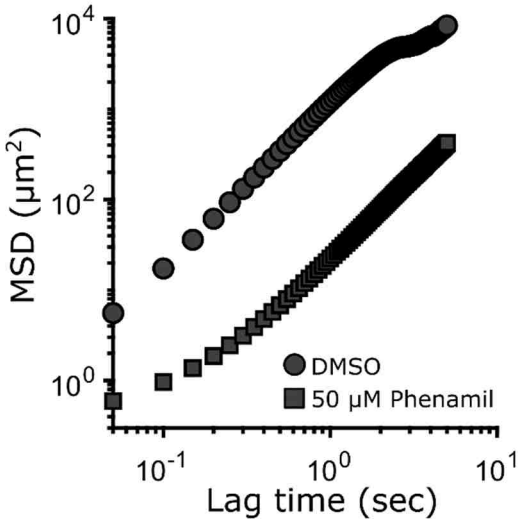

Extended Data Fig. 4. **Phenamil inhibits *V. cholerae* motility.** Mean squared displacement (MSD) of cell trajectories versus lag time for WT *V. cholerae* treated with DMSO solvent or 50 μM phenamil.

Supplemental Discussion

DbfS is not equivalent to PhoQ

In *E. coli*, low Mg^{2+} and cationic peptides activate PhoQ kinase activity.[40] Sequence alignment of the DbfS sensory domain with that from PhoQ of *E. coli*, *Salmonella enterica*, and *Pseudomonas aeruginosa* revealed that DbfS lacks all of the key residues involved in Mg^{2+} binding (Extended Data Fig. 2A).[41] To test if Mg^{2+} alters DfbS activity, we measured the *V. cholerae* biofilm lifecycle in response to low Mg^{2+} conditions in WT *V. cholerae* and in the Δ*dbfR* mutant. If, analogous to PhoQ, DfbS kinase activity is activated by low Mg^{2+}, when Mg^{2+} is limiting, WT *V. cholerae* should exhibit an altered biofilm dispersal phenotype while the Δ*dbfR* mutant would be impervious to Mg^{2+} changes.[40] Extended Data Fig. 2B shows that Mg^{2+} limitation does indeed inhibit *V. cholerae* biofilm dispersal, however, inhibition occurs in *both* the WT and the Δ*dbfR* strains. Mg^{2+} limitation did not alter *vpsL-lux* expression in either strain (Extended Data Fig. 2C). Thus, Mg^{2+} does not control DfbS activity. We obtained the same results following exogenous addition of the cationic peptide C18G (Extended Data Fig. 2D). Together, these results demonstrate that DfbS does not respond to the ligands that control PhoQ activity.

Acknowledgements

We thank members of the Bassler group and Prof. Ned Wingreen for thoughtful discussions. We particularly thank Dr. Matthew Jemielita for help with the secreted protease mutants used in this study. This work was supported by the Howard Hughes Medical Institute, NIH Grant 5R37GM065859, National Science Foundation Grant MCB-1713731, and a Max Planck-Alexander von Humboldt research award to BLB. AAB is a Howard Hughes Medical Institute Fellow of the Damon Runyon Cancer Research Foundation, DRG-2302-17. The content is solely the responsibility of the authors and does not necessarily represent the official views of the National Institutes of Health. The funders had no role in study design, data collection and analysis, decision to publish, or preparation of the manuscript.

Supplementary Table 1

Strains used in this study.

Strain Number	Genotype	Plasmid	Antibiotic Resistance	Parent
BB_Vc_0090	WT O1 El Tor biotype C6706str2	-	Sm	-
AB_Vc_761	Δ*vc1807*::Cm^R (Referred to as WT)	-	Sm, Cm	BB_Vc_0090
AB_Vc_705	Δ*cheY* Δ*vc1807*::Cm^R	-	Sm, Cm	BB_Vc_0090
AB_Vc_708	Δ*bipA* Δ*vc1807*::Cm^R	-	Sm, Cm	BB_Vc_0090
AB_Vc_839	Δ*mbaA* Δ*vc1807*::Cm^R	-	Sm, Cm	BB_Vc_0090
AB_Vc_711	Δ*potD1* Δ*vc1807*::Cm^R	-	Sm, Cm	BB_Vc_0090
AB_Vc_757	Δ*lapG* Δ*vc1807*::Cm^R	-	Sm, Cm	BB_Vc_0090
AB_Vc_758	Δ*rocS* Δ*vc1807*::Cm^R	-	Sm, Cm	BB_Vc_0090
AB_Vc_775	Δ*dbfS* Δ*vc1807*::Cm^R	-	Sm, Cm	BB_Vc_0090
AB_Vc_777	Δ*cdgI* Δ*vc1807*::Cm^R	-	Sm, Cm	BB_Vc_0090
AB_Vc_778	Δ*cdgG* Δ*vc1807*::Cm^R	-	Sm, Cm	BB_Vc_0090
AB_Vc_485	Δ*rbmB* Δ*vc1807*::Kan^R	-	Sm, Kan	BB_Vc_0090
AB_Vc_801	Δ*vc1807*::Kan^R	pEVS143-P_{vpsL}-*lux*::Cm^R	Sm, Cm, Kan	AB_Vc_479
AB_Vc_825	Δ*cheY* Δ*vc1807*::Kan^R	pEVS143-P_{vpsL}-*lux*::Cm^R	Sm, Cm, Kan	AB_Vc_705
AB_Vc_829	Δ*lapG* Δ*vc1807*::Kan^R	pEVS143-P_{vpsL}-*lux*::Cm^R	Sm, Cm, Kan	AB_Vc_757
AB_Vc_802	Δ*rbmB* Δ*vc1807*::Kan^R	pEVS143-P_{vpsL}-*lux*::Cm^R	Sm, Cm, Kan	AB_Vc_485
AB_Vc_815	Δ*dbfS* Δ*vc1807*::Kan^R	pEVS143-P_{vpsL}-*lux*::Cm^R	Sm, Cm, Kan	AB_Vc_775
AB_Vc_773	Δ*dbfR* Δ*vc1807*::Cm^R	-	Sm, Cm	BB_Vc_0090
AB_Vc_701	Δ*dbfRS* Δ*vc1807*::Cm^R	-	Sm, Cm	BB_Vc_0090
AB_Vc_788	*dbfR*^{D51V} Δ*vc1807*::Cm^R	-	Sm, Cm	BB_Vc_0090
AB_Vc_891	*dbfR*^{D51V} Δ*dbfS* Δ*vc1807*::Kan^R		Sm, Kan	BB_Vc_0090
AB_Vc_863	*dbfR-SNAP* Δ*dbfS* Δ*vc1807*::P_{BAD}-*dbfS*::Spec^R	-	Sm, Spec	BB_Vc_0090
AB_Vc_865	Δ*dbfS* Δ*vc1807*::P_{BAD}-*dbfS*::Spec^R	-	Sm, Spec	BB_Vc_0090
AB_Vc_879	*dbfR-SNAP* Δ*vc1807*::Kan^R	-	Sm, Kan	BB_Vc_0090
AB_Vc_881	*dbfR*^{D51V}*-SNAP* Δ*vc1807*::Kan^R	-	Sm, Kan	BB_Vc_0090
AB_Vc_859	Δ*lapG* Δ*vc1807*::P_{BAD}-*lapG*::Spec^R	-	Sm, Spec	AB_Vc_757
AB_Vc_898	Δ*lapD* Δ*vc1807*::Kan^R	-	Sm, Kan	BB_Vc_0090
AB_Vc_900	Δ*lapD* Δ*lapG* Δ*vc1807*::Kan^R	-	Sm, Kan	BB_Vc_0090
AB_Vc_862	Δ*rbmB* Δ*vc1807*::P_{BAD}-*rbmB*::Spec^R	-	Sm, Spec	AB_Vc_485
BB_Vc_0252	Δ*dns*	-	Sm	BB_Vc_0090
BB_Vc_0253	Δ*xds*	-	Sm	BB_Vc_0090
BB_Vc_0254	Δ*dns* Δ*xds*	-	Sm	BB_Vc_0090
MJ_552	Δ*hapA* Δ*vc1807*::Kan^R	-	Sm, Kan	BB_Vc_0090
MJ_553	Δ*prtV* Δ*vc1807*::Kan^R	-	Sm, Kan	BB_Vc_0090
MJ_554	Δ*vesA* Δ*vc1807*::Kan^R	-	Sm, Kan	BB_Vc_0090
MJ_555	Δ*vesB* Δ*vc1807*::Kan^R	-	Sm, Kan	BB_Vc_0090
MJ_562	Δ*vesC* Δ*vc1807*::Kan^R	-	Sm, Kan	BB_Vc_0090

MJ_561	Δ*lap* Δ*lapX lacZ*::*Ptac-mKO* Δ*vc1807*::Kan^{R}	-	Sm, Kan	BB_Vc_0090
AB_Vc_792	Δ*tagA* Δ*vc1807*::Cm^{R}	-	Sm, Cm	BB_Vc_0090
AB_Vc_715	*cheY*$^{D16K, Y109W}$ Δ*vc1807*::Kan^{R}	-	Sm, Kan	BB_Vc_0090
AB_Vc_732	Δ*vpsL* Δ*vc1807*::*Ptac-mScarletI*::Spec^{R}	-	Sm, Spec	BB_Vc_0090
AB_Vc_735	Δ*cheY* Δ*vpsL* Δ*vc1807*::*Ptac-mScarletI*::Spec^{R}	-	Sm, Spec	AB_Vc_705
AB_Vc_745	*cheY*$^{D16K, Y109W}$ Δ*vpsL* Δ*vc1807*::*Ptac-mScarletI*::Spec^{R}	-	Sm, Spec	AB_Vc_715

Supplementary Table 2

DNA oligonucleotides and gene fragments used in this study.

Oligo #	Name	Purpose	Direction	5' to 3' Sequence
551	*cheY*_3000up	Cloning at *cheY3* locus	F	CAAGCGTTACAACTCGCAGCCTAG
552	*cheY*_3000down	Cloning at *cheY3* locus	R	CACAACCAGACCTACGCGCTGAC
553	*cheY*_100up	Cloning at *cheY3* locus	F	GGTGAGGTACTTGGAGTTAGTGAATCTC
554	*cheY*_100down	Cloning at *cheY3* locus	R	CACTGAAGCGCTCATCAATCTGAAAG
555	*cheY*_B	*cheY3* deletion	R	GAGCACCTTTTGCCGCAGCAAAAGCCTGAGTTTGAGATCAG TGATATTTAGTCATTCC
556	*cheY*_C	*cheY3* deletion	F	GGAATGACTAAATATCACTGATCTCAAACTCAGGCTTTTGCT GCGGCAAAAGGTGCTC
561	*cheY*_2700up	Cloning at *cheY3* locus	F	GATGACCGTGTCAGTTTGCAATCGAG
562	*cheY*_2700down	Cloning at *cheY3* locus	R	CTTCGGTGCTAACCAGTTTTGTAAG*TAGA*AC
563	*cheY*_up_R	Cloning at *cheY3* locus	R	GAGTTTGAGATCAGTGATATTTAGTCATTCCGAGTCC
564	*cheY*_down_R	Cloning at *cheY3* locus	R	GGCTTTTGCTGCGGCAAAAGGTGCTCTATTC
566	*cheY*_D16K_Y109W	Gblock for introduction of *cheY3* point mutation	F	GTTAAGTTCTTGGACTCGGAATGACTAAATATCACTGATCTC AAACTCAGTGGAGGCAATTTTGAATAAAAACATGAAGATCCT TATTGTTGATAAGTTTTCAACAATGCGCCGAATCGTTAAAAA CCTACTTCGAGATCTGGGGTTCAATAACACGCAGGAAGCGG ACGATGGCCTAACGGCATTGCCTATGCTCAAGAAAGGTGAT TTTGACTTTGTAGTCACAGACTGGAATATGCCCGGTATGCAA GGTATTGACTTGCTTAAAAATATCCGTGCCGACGAAGAACTG AAGCACCTGCCTGTACTAATGATCACAGCAGAAGCCAAACG TGAGCAAATCATCGAAGCCGCTCAAGCAGGCGTGAATGGTT GGATCGTAAAACCATTTACCGCTGCTACGCTTAAAGAAAAAT *TAGA*CAAAATTTTTGAGCGTTTATAAGGCTTTTGCTGCGGCA AAAGGTGCTCTATTCACACGCGCAAAAG
545	*bipA*_3000up	Cloning at *bipA* locus	F	GCTGCGTGAGCAGTTGTAAATCGAG
546	*bipA*_3000down	Cloning at *bipA* locus	R	CAACGCTTTGTAGTTCGGGATTAGCATATA
547	*bipA*_100up	Cloning at *bipA* locus	F	GTCGACGATTTCAGCGCGACAGATC
548	*bipA*_100down	Cloning at *bipA* locus	R	GAGGTATTTCTGGATAGGTGGCATAGC
549	*bipA*_B	*bipA* deletion	R	GATGACTTATCTTACCAAACGAAAGTCAGTGACGGGGTTTG CTTCACTTTTTCATTGAGGCTG
550	*bipA*_C	*bipA* deletion	F	CAGCCTCAATGAAAAAGTGAAGCAAACCCCGTCACTGACTT TCGTTTGGTAAGATAAGTCATC
567	*bipA*_2700up	Cloning at *bipA* locus	R	CAGTGACTCGTCCAAAATGAGCACTG
568	*bipA*_2700down	Cloning at *bipA* locus	R	GATCTAAATCGCCACTGATCCCATCAAG
571	*mbaA*_3000up	Cloning at *mbaA* locus	F	GCGCGCTAATCTGAACTCAACCCATAAG
572	*mbaA*_2700up	Cloning at *mbaA* locus	F	CGTTAGCATTCCACGCGGTCAGTTAG
711	*mbaA*_KO2_B	*mbaA* deletion	R	GGAGGCATGAAGCCATGGGGAGATCTCGCTATGGTTTAGCT TCATATTGGTAAGTCACACTG
712	*mbaA*_KO2_C	*mbaA* deletion	F	CAGTGTGACTTACCAATATGAAGCTAAACCATAGCGAGATCT CCCCATGGCTTCATGCCTCC
575	*mbaA*_2700down	Cloning at *mbaA* locus	R	GATCTCATGACGCGCCTGACGGTATTTAAG
576	*mbaA*_3000down	Cloning at *mbaA* locus	R	CATCGTTCGCGATAGTGGGAAATTCAATAAAATG

577	*mbaA*_100up	Cloning at *mbaA* locus	F	GAAACCTGACATTGCCGCAATCAATGC
578	*mbaA*_100down	Cloning at *mbaA* locus	R	CCTGCTTCCAATCCGACATAATACTCTGC
539	*potD1*_3000up	Cloning at *potD1* locus	F	CTGGAATCCGGTATGTGTGTGATGGTTAG
540	*potD1*_3000down	Cloning at *potD1* locus	R	AGAGCGACTAGGTGTTATTGAACTTGGG
541	*potD1*_100up	Cloning at *potD1* locus	F	CTAAGAAAAGCATCAAATAGGCAGCCATTG
542	*potD1*_100down	Cloning at *potD1* locus	R	GATCTGGAAGAGATTAAGGCGCTCTC
543	*potD1*_B	*potD1* deletion	R	GGTGGCTTTTTAATGGGAGATAAAAGGCTACGTTCCCATAGTGTA*TAGA*AAGAACC
544	*potD1*_C	*potD1* deletion	F	GGTTCTTTCTATACACTATGGGAACGTAGCCTTTTATCTCCCATTAAAAAGCCACC
569	*potD1*_2700up	Cloning at *potD1* locus	F	CTGATGATTATTGGTACGAGTTTTCTGACTCGTG
570	*potD1*_2700down	Cloning at *potD1* locus	R	CGATAATCCAAATCAAATCGAGGTGCAGG
602	*lapG*_3000up	Cloning at *lapG* locus	F	CAAACAATTACCCGGTTATTGGGGATG
603	*lapG*_2700up	Cloning at *lapG* locus	F	GCATTCCGTCAAAGTGCTCGATATTCATC
604	*lapG*_100up	Cloning at *lapG* locus	F	GATCATTCCGGGAATGACCGCTTC
605	*lapG*_B	Cloning at *lapG* locus	R	CGACTAGTTGTTTGTATAGCGTCATAGTGCAGGGCGGGCTATTCCCTCAGCGCATTGCTTTG
606	*lapG*_C	*lapG* deletion	F	CAAAGCAATGCGCTGAGGGAATAGCCCGCCCTGCACTATGACGCTATACAAACAACTAGTCG
607	*lapG*_100down	*lapG* deletion	R	GTGTTGTTGACTTCAGAGCGTTGTTG
608	*lapG*_2700down	Cloning at *lapG* locus	R	GTCCAGCCATTAACCAGATCAACAC
609	*lapG*_3000down	Cloning at *lapG* locus	R	CAGCGGTACTGGAATTGTCCTTGC
774	*lapD*_3000up	Cloning at *lapD* locus	F	CGCGAATACAAGAAGCGATCATGCAG
775	*lapD*_2700up	Cloning at *lapD* locus	F	GCAAACTTCTGCTTAAGCTCAAGATACTTGC
776	*lapD*_100up	Cloning at *lapD* locus	F	CAATTGGCTGGGGACTCTTCGAGAC
777	*lapD*_B	*lapD* deletion	R	GTATCTTGCATGCCTCTGACCTTGGAGTGCCTACTCATCATAGCTAAC
778	*lapD*_C	*lapD* deletion	F	GTTAGCTATGATGAGTAGGCACTCCAAGGTCAGAGGCATGCAAGATAC
779	*lapD*_100down	Cloning at *lapD* locus	R	GTAAGCCGTTGATCAGTGCTTCAGGAG
780	*lapD*_2700down	Cloning at *lapD* locus	R	CTAACTACGCGCAGTATGTTGAGTTACAAGCG
781	*lapD*_3000down	Cloning at *lapD* locus	R	CGTTCAAGCACAAGGCGATA*TAGA*CG
784	*lapDG*_B	*lapDG* deletion	R	GTATCTTGCATGCCTCTGACCTTGGAGGGCGGGCTATTCCCTCAGCGCATTG
785	*lapDG*_C	*lapDG* deletion	F	CAATGCGCTGAGGGAATAGCCCGCCCTCCAAGGTCAGAGGCATGCAAGATAC
610	*rocS*_3000up	Cloning at *rocS* locus	F	CAACTCGAGCTTTTCTACCAACCTCAG
611	*rocS*_2700up	Cloning at *rocS* locus	F	GCATTTTACCGCCCCATTTTCGC
612	*rocS*_100up	Cloning at *rocS* locus	F	CTTCAGGCCAAGATCCTTTTCTACTGTG
613	*rocS*_B	*rocS* deletion	R	GGTTTCCACCAATCAGAGTAAAATTAACCCCTTAAAATACTACCAACTGTCCGTGCGCGACGACG
614	*rocS*_C	*rocS* deletion	F	CGTCGTCGCGCACGGACAGTTGGTAGTATTTTAAGGGGTTAATTTTACTCTGATTGGTGGAAACC

615	*rocS*_100down	Cloning at *rocS* locus	R	GAAACCGATATAAACCGCATCGGCA
616	*rocS*_2700down	Cloning at *rocS* locus	R	GTCACGTTATTAGGCTTGGCGTATTTC
617	*rocS*_3000down	Cloning at *rocS* locus	R	GCTGTTTGTTCACCTTAGGCTCG
533	*vc1639*_3000up	Cloning at *dbfS* locus	F	GCTTAGTGATCGCAGAGCTTGC
534	*vc1639*_3000down	Cloning at *dbfS* locus	R	GTGCACTGCATTATTGACTCGCTTAGC
535	*vc1639*_100up	Cloning at *dbfS* locus	F	CAAGATTTTGACCGCGATTCCAATAC
536	*vc1639*_100down	Cloning at *dbfS* locus	R	G*TAGA*GTTTCCAAACCTATAGGAG
626	*vc1639*_Real_B	*dbfS* deletion	R	CAACTGAAAATCCGTTTTTGCACCGCATTTAATTGGCATGCA ACTGATACCCAAG
627	*vc1639*_Real_C	*dbfS* deletion	F	CTTGGGTATCAGTTGCATGCCAATTAAATGCGGTGCAAAAAC GGATTTTCAGTTG
559	*vc1639*_2700up	Cloning at *dbfS* locus	F	CAATCGGTGGTGCGCAACTTATCTGAG
560	*vc1639*_2700down	Cloning at *dbfS* locus	R	GTTAATGACTTGGAGCAGAATTAAGTTAGCCGC
527	*vc1638*_3000up	Cloning at *dbfR* locus	F	GTAGGTCTTCTCGCACTTGTGTTTTG
528	*vc1638*_3000down	Cloning at *dbfR* locus	R	GTCCATAACCTTAGCGGAACTCATG
529	*vc1638*_100up	Cloning at *dbfR* locus	F	GACAATCAAGTCTTTCGTGTCGAATACAAC
530	*vc1638*_100down	Cloning at *dbfR* locus	R	CTTCCAGCAAATATTGATGGATGAGATTTGGG
628	*vc1638*_Real_B	*dbfR* deletion	R	GAGATTTAATTGGCATGCAACTGATACCCAAGGTCTGCTCG ATTATTTTTTGATGGCACG
629	*vc1638*_Real_C	*dbfR* deletion	F	CGTGCCATCAAAAAATAATCGAGCAGACCTTGGGTATCAGTT GCATGCCAATTAAATCTC
557	*vc1638*_2700up	Cloning at *dbfR* locus	F	CACCATCCGGTTTGTGCATCATGATG
558	*vc1638*_2700down	Cloning at *dbfR* locus	R	GTGGCGTCAGATCCCAAAACTTGTTC
650	*dbfR*_D51V_B	Generating $dbfR^{D51V}$	R	CAATTTCGGTAGGCCGAGTACGAGTACGATGACGTCC
651	*dbfR*_D51V_C	Generating $dbfR^{D51V}$	F	GGACGTCATCGTACTCGTACTCGGCCTACCGAAATTG
736	*dbfR*_SNAP_delta S_Gblock	Gblock for generating *dbfR-SNAP* and simultaneously deleting *dbfS*	F	CGCGGTCTTGGGTATCAGTTGCATGCCAATTCAGGAAGCGG CTCAGGCAGCGGATCAGGAATGGATAAGGATTGTGAAATGA AGAGAACAACTT*TAGA*TTCCCCACTAGGTAAAT*TAGA*ATTAT CCGGTTGCGAACAAGGATTACATCGTATTATATTTTTAGGAA AAGGAACCAGTGCAGCAGACGCCG*TAGA*AGTACCAGCCCC CGCCGCAGTTTTAGGAGGACCAGAACCACTAATGCAAGCCA CCGCTTGGTTAAACGCATATTTTCATCAACCAGAAGCCA*TAG A*AGAATTCCCAGTACCAGCCCTACACCACCCAGTATTTCAAC AAGAATCATTTACGAGACAAGTATTATGGAAATTATTAAAAGT CGTCAAATTCGGAGAAGTTATCAGCTATAGTCACCTAGCCG CTCTTGCCGGTAATCCAGCAGCCACTGCCGCAGTTAAAACC GCATTATCAGGTAACCCAGTTCCCATATTAATTCCATGCCA*T AGA*GTAGTACAAGGAGATT*TAGA*CGTCGGCGGATATGAAGG AGGTTTAGCAGTTAAAGAATGGTTACTAGCACATGAAGGACA *TAGA*TTAGGTAAACCAGGATTAGGTTAAATGCGGTGCAAAAA CGGATTTTCAGTTGC
734	*dbfR*_R	Generating *dbfR-SNAP* and deleting *dbfS*	R	TTGGCATGCAACTGATACCCAAGACCGCG
735	*dbfS*_down_F	Generating *dbfR-SNAP* and deleting *dbfS*	F	ATGCGGTGCAAAAACGGATTTTCAGTTGC
672	SNAP_UnivR	Generating *dbfR-SNAP*	R	TTAACCTAATCCTGGTTTACCTAATCTATGTCCTTCATGTGCT AGTAACC

718	*dbfR*_SNAP_E	Generating *dbfR*-SNAP	F	GACA*TAGA*TTAGGTAAACCAGGATTAGGTTAAGATGTGATCAAAACTGTGCGCGGTC
634	*cdgI*_3000up	Cloning at *cdgI* locus	F	CGATGCAAGTAGCTGAACAAGCAC
635	*cdgI*_2700up	Cloning at *cdgI* locus	F	GAATACATTGACGCCGAGCGCTTTG
636	*cdgI*_100up	Cloning at *cdgI* locus	F	GGGAGCAACTTCACTGTATTCAATGAGTG
637	*cdgI*_B	*cdgI* deletion	R	GATGCGATCATCATGAGCTACCTATTTTTGTAAAGGCCCGACTTCATTTTTTTCTACTCTC
638	*cdgI*_C	*cdgI* deletion	F	GAGAG*TAGA*AAAAAATGAAGTCGGGCCTTTACAAAAATAGGTAGCTCATGATGATCGCATC
639	*cdgI*_100down	Cloning at *cdgI* locus	R	GGTCAGCAGCTTTTGCAGCACTTTATTG
640	*cdgI*_2700down	Cloning at *cdgI* locus	R	GAGGTGCAACCTGCGTGTAACTGGATTTTC
641	*cdgI*_3000down	Cloning at *cdgI* locus	R	CCAGTGAGGCTATCAATATGCGCATC
642	*cdgG*_3000up	Cloning at *cdgG* locus	F	GTGTCGATTCCAGCGACAAGTGCCAATTTG
643	*cdgG*_2700up	Cloning at *cdgG* locus	F	GAATACACCGCAGAGCCGATAGTGAC
644	*cdgG*_100up	Cloning at *cdgG* locus	F	GATAAATGCTGCCCAGTCGGCATAAACACTGAG
645	*cdgG*_B	*cdgG* deletion	R	GCACAAATTAATAGTTAATTAGCTTAAATATTAATCAGACTGGATAGTTGAGGATCAATCCTGATCC
646	*cdgG*_C	*cdgG* deletion	F	GGATCAGGATTGATCCTCAACTATCCAGTCTGATTAATATTTAAGCTAATTAACTATTAATTTGTGC
647	*cdgG*_100down	Cloning at *cdgG* locus	R	TTGAGGCCATGC*TAGA*GCATGATGTTGAGC
648	*cdgG*_2700down	Cloning at *cdgG* locus	R	CCAGTAAATTCGGGTTATGAGGTAAAGGATG
649	*cdgG*_3000down	Cloning at *cdgG* locus	R	GATCGCCACTTTCCGCGATTGGATG
105	BBC1881	Cloning at *vc1807* locus	F	TTTAAAGGGGATCAGTGACCG
106	BBC1882	Cloning at *vc1807* locus	R	CAATTTTGCTTTTGGACCATCCC
270	*1807*_2700up	Cloning at *vc1807* locus	F	GGCCGGCACTTTGATTACAATC
271	*1807*_2700down	Cloning at *vc1807* locus	R	GTCTATATCAGAGCGCTTAAAGAGCG
721	P_{BAD}*_1807*_Univ_B	Generating P_{BAD}-*dbfS*	R	CATTTCACACCTCCTGCAGGTAC
722	P_{BAD}-*dbfS-1807*_C	Generating P_{BAD}-*dbfS*	F	GTACCTGCAGGAGGTGTGAAATGGGTATCAGTTGCATGCCAATTAAATCTCG
723	P_{BAD}-*dbfS-1807*_D	Generating P_{BAD}-*dbfS*	R	GTCGACGGATCCCCGGAATTTAATGGGATTTGACGGCTTTGGCTG
232	ABD123	Generating P_{BAD}-*dbfS*	F	ATTCCGGGGATCCGTCGAC
729	P_{BAD}-*lapG-1807*_C	Generating P_{BAD}-*lapG*	R	GTACCTGCAGGAGGTGTGAAATGAAACGTTGGATTGTGCTGTCTCTGG
730	P_{BAD}-*lapG-1807*_D	Generating P_{BAD}-*lapG*	F	GTCGACGGATCCCCGGAATCTACTCATCATAGCTAAC*TAGA*GG
731	P_{BAD}-*rbmB-1807*_C	Generating P_{BAD}-*rbmB*	R	GTACCTGCAGGAGGTGTGAAATGCTGTTATACTTAAATCAATTCAATAAAGAGGGTGG
732	P_{BAD}-*rbmB-1807*_D	Generating P_{BAD}-*rbmB*	F	GTCGACGGATCCCCGGAATTCAATCTTTAATAAAGTGCTGTATATAATAATGGTCGC
587	*tagA*_3000up	Cloning at *tagA* locus	F	GGGCTGCAAGAACTGGATCTGCTAC
588	*tagA*_2700up	Cloning at *tagA* locus	F	GAGCAAAATTACAAGCTCGATCTTCAGCTAAG
662	*tagA*_103bpD_B	Removes first 103 codons of	R	GTCAAATACTGGTCGTTACTGGATGTTGCATTCTTTAACAAAAAAATAAAGACAAGGGAAACGTATTG

		tagA including start		
663	*tagA*_103bpD_C	Removes first 103 codons of *tagA* including start	F	CAATACGTTTCCCTTGTCTTTATTTTTTTGTTAAAGAATGCAA CATCCAGTAACGACCAGTATTTGAC
591	*tagA*_2700down	Cloning at *tagA* locus	R	CCACCGAGGATACCATCCATCTTGATAATATG
592	*tagA*_3000down	Cloning at *tagA* locus	R	CTCTTGCCATCCATATGACATGATGTCTTTTG
593	*tagA*_100up	Cloning at *tagA* locus	F	GTGTGGCTTCATCCATTGACCTCCAATG
594	*tagA*_100down	Cloning at *tagA* locus	R	CCACTGCGAAATTAATTTTAGGATCAGCTTTAGC
664	*tagA*_150down	Cloning at *tagA* locus	R	GCAACCATACATCTTCCATTACTACCATAAGAG

References

1. Matz, C. *et al.* Biofilm formation and phenotypic variation enhance predation-driven persistence of Vibrio cholerae. *PNAS* **102**, 16819–16824 (2005).
2. Yan, J. & Bassler, B. L. Surviving as a community: antibiotic tolerance and persistence in bacterial biofilms. *Cell Host Microbe* **26**, 15–21 (2019).
3. Shaw, T., Winston, M., Rupp, C. J., Klapper, I. & Stoodley, P. Commonality of elastic relaxation times in biofilms. *Phys. Rev. Lett.* **93**, 098102 (2004).
4. Walter, J., Britton, R. A. & Roos, S. Host-microbial symbiosis in the vertebrate gastrointestinal tract and the Lactobacillus reuteri paradigm. *PNAS* **108**, 4645–4652 (2011).
5. Roilides, E., Simitsopoulou, M., Katragkou, A. & Walsh, T. J. How biofilms evade host defenses. *Microbiology Spectrum* **3**, (2015).
6. Mah, T. F. & O'Toole, G. A. Mechanisms of biofilm resistance to antimicrobial agents. *Trends Microbiol.* **9**, 34–39 (2001).
7. Phillips, P. L. & Schultz, G. S. Molecular mechanisms of biofilm infection: biofilm virulence factors. *Adv Wound Care (New Rochelle)* **1**, 109–114 (2012).
8. Guilhen, C., Forestier, C. & Balestrino, D. Biofilm dispersal: multiple elaborate strategies for dissemination of bacteria with unique properties. *Mol. Microbiol.* **105**, 188–210 (2017).
9. Hobley, L., Harkins, C., MacPhee, C. E. & Stanley-Wall, N. R. Giving structure to the biofilm matrix: an overview of individual strategies and emerging common themes. *FEMS Microbiol Rev* **39**, 649–669 (2015).
10. Conner, J. G., Teschler, J. K., Jones, C. J. & Yildiz, F. H. Staying alive: Vibrio cholerae's cycle of environmental survival, transmission, and dissemination. *Microbiol Spectr* **4**, (2016).
11. Almagro-Moreno, S., Pruss, K. & Taylor, R. K. Intestinal colonization dynamics of Vibrio cholerae. *PLOS Pathogens* **11**, e1004787 (2015).
12. Silva, A. J. & Benitez, J. A. Vibrio cholerae biofilms and cholera pathogenesis. *PLOS Neglected Tropical Diseases* **10**, e0004330 (2016).
13. Gallego-Hernandez, A. L. *et al.* Upregulation of virulence genes promotes Vibrio cholerae biofilm hyperinfectivity. *Proc. Natl. Acad. Sci. U.S.A.* **117**, 11010–11017 (2020).
14. Tamayo, R., Patimalla, B. & Camilli, A. Growth in a Biofilm induces a hyperinfectious phenotype in Vibrio cholerae. *Infection and Immunity* **78**, 3560–3569 (2010).
15. Valentini, M. & Filloux, A. Biofilms and Cyclic di-GMP (c-di-GMP) Signaling: lessons from Pseudomonas aeruginosa and other bacteria. *J Biol Chem* **291**, 12547–12555 (2016).
16. Conner, J. G., Zamorano-Sánchez, D., Park, J. H., Sondermann, H. & Yildiz, F. H. The ins and outs of cyclic di-GMP signaling in Vibrio cholerae. *Curr Opin Microbiol* **36**, 20–29 (2017).
17. Fong, J. C. N., Syed, K. A., Klose, K. E. & Yildiz, F. H. Role of Vibrio polysaccharide (vps) genes in VPS production, biofilm formation and Vibrio cholerae pathogenesis. *Microbiology (Reading, Engl.)* **156**, 2757–2769 (2010).
18. Bridges, A. A. & Bassler, B. L. The intragenus and interspecies quorum-sensing autoinducers exert distinct control over Vibrio cholerae biofilm formation and dispersal. *PLoS Biol.* **17**, e3000429 (2019).
19. Singh, P. K. *et al.* Vibrio cholerae combines individual and collective sensing to trigger biofilm dispersal. *Curr Biol* **27**, 3359-3366.e7 (2017).
20. Merrell, D. S., Hava, D. L. & Camilli, A. Identification of novel factors involved in colonization and acid tolerance of Vibrio cholerae. *Molecular Microbiology* **43**, 1471–1491 (2002).
21. Gao, R. & Stock, A. M. Biological insights from structures of two-Component proteins. *Annu Rev Microbiol* **63**, 133–154 (2009).
22. Gao, R., Bouillet, S. & Stock, A. M. Structural basis of response regulator function. *Annu. Rev. Microbiol.* **73**, 175–197 (2019).

23. Boyd, C. D., Chatterjee, D., Sondermann, H. & O'Toole, G. A. LapG, required for modulating biofilm formation by Pseudomonas fluorescens Pf0-1, is a calcium-dependent protease. *Journal of Bacteriology* **194**, 4406–4414 (2012).
24. Fong, J. C. N. & Yildiz, F. H. The rbmBCDEF gene cluster modulates development of rugose colony morphology and biofilm formation in Vibrio cholerae. *Journal of Bacteriology* **189**, 2319–2330 (2007).
25. Kitts, G. *et al.* A conserved regulatory circuit controls large adhesins in Vibrio cholerae. *mBio* **10**, (2019).
26. Collins, A. J., Smith, T. J., Sondermann, H. & O'Toole, G. A. From input to output: the lap/c-di-GMP biofilm regulatory circuit. *Annu. Rev. Microbiol.* (2020).
27. Berk, V. *et al.* Molecular architecture and assembly principles of Vibrio cholerae biofilms. *Science* **337**, 236–239 (2012).
28. Seper, A. *et al.* Extracellular nucleases and extracellular DNA play important roles in Vibrio cholerae biofilm formation. *Mol Microbiol* **82**, 1015–1037 (2011).
29. Hyakutake, A. *et al.* Only one of the five cheY homologs in Vibrio cholerae directly switches flagellar rotation. *Journal of Bacteriology* **187**, 8403–8410 (2005).
30. Butler, S. M. & Camilli, A. Going against the grain: chemotaxis and infection in Vibrio cholerae. *Nat Rev Microbiol* **3**, 611–620 (2005).
31. Butler, S. M. & Camilli, A. Both chemotaxis and net motility greatly influence the infectivity of Vibrio cholerae. *Proc Natl Acad Sci U S A* **101**, 5018–5023 (2004).
32. Son, K., Guasto, J. S. & Stocker, R. Bacteria can exploit a flagellar buckling instability to change direction. *Nature Physics* **9**, 494–498 (2013).
33. Licata, N. A., Mohari, B., Fuqua, C. & Setayeshgar, S. Diffusion of bacterial cells in porous media. *Biophys J* **110**, 247–257 (2016).
34. Utada, A. S. *et al.* Vibrio cholerae use pili and flagella synergistically to effect motility switching and conditional surface attachment. *Nature Communications* **5**, 4913 (2014).
35. Wu, D. C. *et al.* Reciprocal c-di-GMP signaling: incomplete flagellum biogenesis triggers c-di-GMP signaling pathways that promote biofilm formation. *PLOS Genetics* **16**, e1008703 (2020).
36. Kojima, S., Yamamoto, K., Kawagishi, I. & Homma, M. The polar flagellar motor of vibrio cholerae is driven by an Na+ motive force. *J Bacteriol* **181**, 1927–1930 (1999).
37. Dalia, A. B., McDonough, E. & Camilli, A. Multiplex genome editing by natural transformation. *Proc Natl Acad Sci U S A* **111**, 8937–8942 (2014).
38. Yan, J. *et al.* Mechanical instability and interfacial energy drive biofilm morphogenesis. *eLife* **8**, e43920 (2019).
39. Qin, B. *et al.* Cell position fates and collective fountain flow in bacterial biofilms revealed by light-sheet microscopy. *Science* (2020).
40. Groisman, E. A. The pleiotropic two-component regulatory system PhoP-PhoQ. *Journal of Bacteriology* **183**, 1835–1842 (2001).
41. Prost, L. R., Daley, M. E., Bader, M. W., Klevit, R. E. & Miller, S. I. The PhoQ histidine kinases of Salmonella and Pseudomonas spp. are structurally and functionally different: evidence that pH and antimicrobial peptide sensing contribute to mammalian pathogenesis. *Mol Microbiol* **69**, 503–519 (2008).

Figures

Figure 1

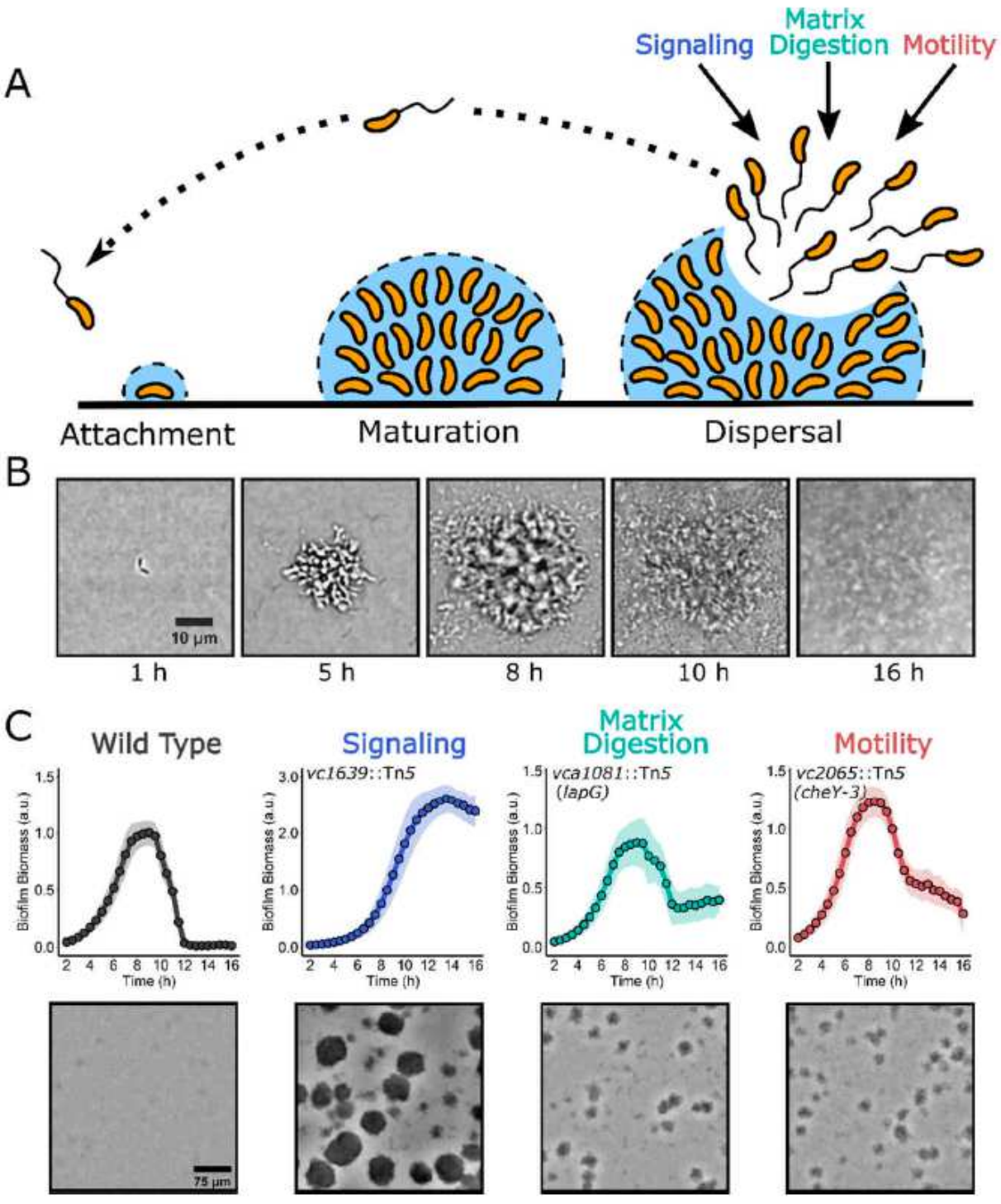

Figure 1

A high-content imaging screen identifies genes required for V. cholerae biofilm dispersal. (A) Schematic illustrating the V. cholerae biofilm lifecycle. See text for details. (B) Brightfield image series over time of the WT V. cholerae biofilm lifecycle. (C) Top panels: Quantitation of biofilm biomass over time as

measured by time-lapse microscopy for WT and representative transposon insertion mutants from each of the three functional categories identified in the screen. Note differences in y-axes scales. Data are represented as means normalized to the peak biofilm biomass of the WT strain. N = 3 biological and N = 3 technical replicates, ± SD (shaded). a.u., arbitrary unit. Bottom panels: Representative brightfield images of biofilms at the final 16 h timepoint for the strains presented in the top panels.

Figure 2

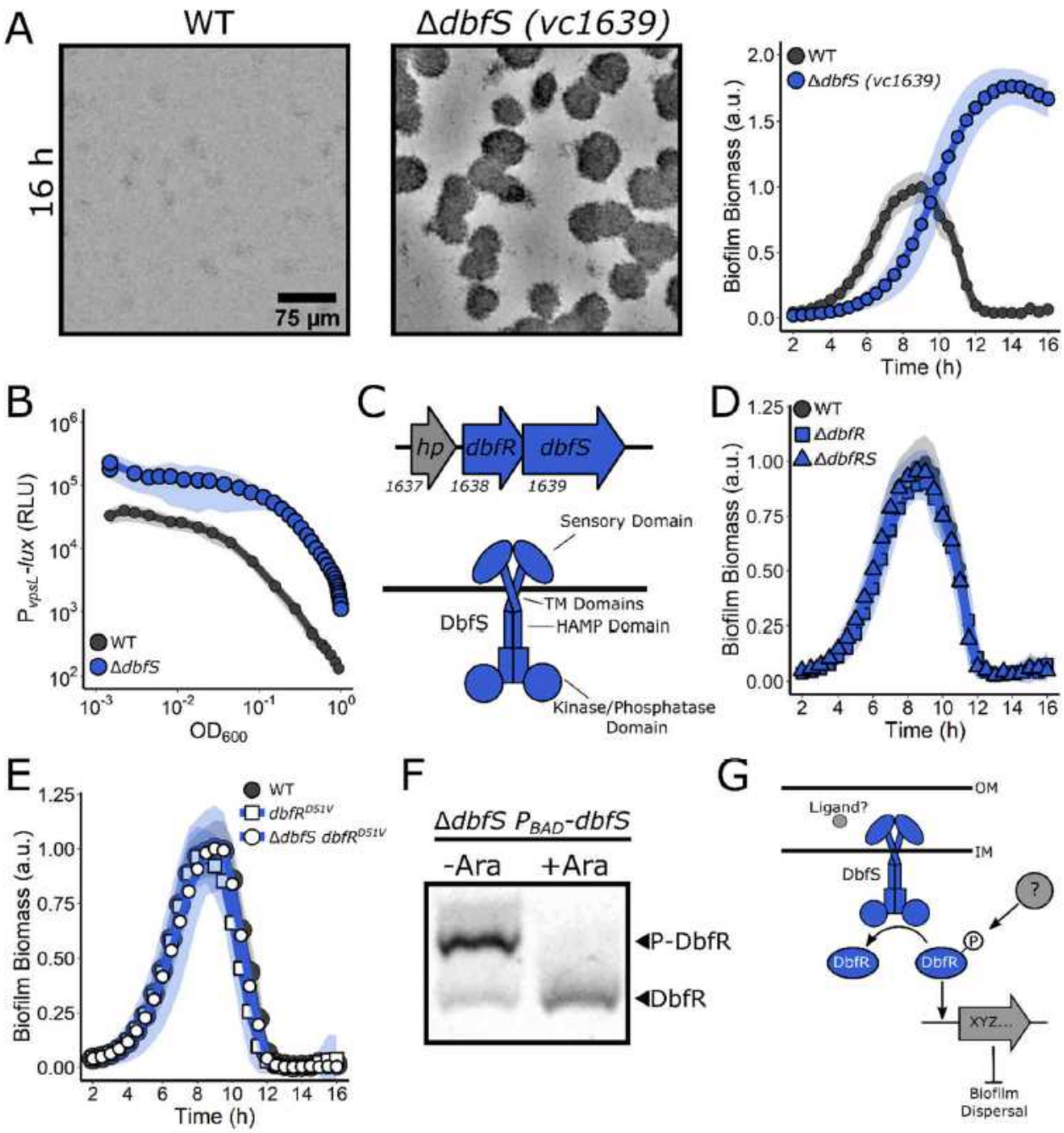

Figure 2

A two-component system that we name DbfS (HK) and DbfR (RR) regulates V. cholerae biofilm dispersal. (A) Representative 16 h images and quantitation of biofilm biomass over time measured by timelapse

microscopy for WT V. cholerae and the ΔdbfS (i.e., Δvc1639) mutant. (B) The corresponding PvpsLlux output for strains and growth conditions in A over the growth curve. (C) Top panel: operon structure of the genes encoding the DbfS-DbfR two-component system. Bottom panel: Cartoon of the domain organization of DbfS. TM, transmembrane domain (D) As in A for the ΔdbfR (i.e., Δvc1638) strain and for the ΔdbfS ΔdbfR double mutant. (E) As in A for the dbfRD51V and ΔdbfS dbfRD51V strains. (F) Representative Phos-tag gel analysis of DbfR-SNAP in the absence (-arabinose) or presence (+arabinose) of DbfS. Fucose was added to repress DbfR production in the uninduced samples. A phosphorylated protein migrates slower than the same unphosphorylated protein. (G) Proposed model for the DbfS-DbfR phosphorylation cascade regulating biofilm dispersal. OM, outer membrane; IM, inner membrane. In all biofilm measurements, N = 3 biological and N = 3 technical replicates, ± SD (shaded). a.u., arbitrary unit. For vpsL-lux measurements, N = 3 biological replicates, ± SD (shaded). RLU, relative light units. Phos-tag gel result is representative of N = 3 biological replicates.

Figure 3

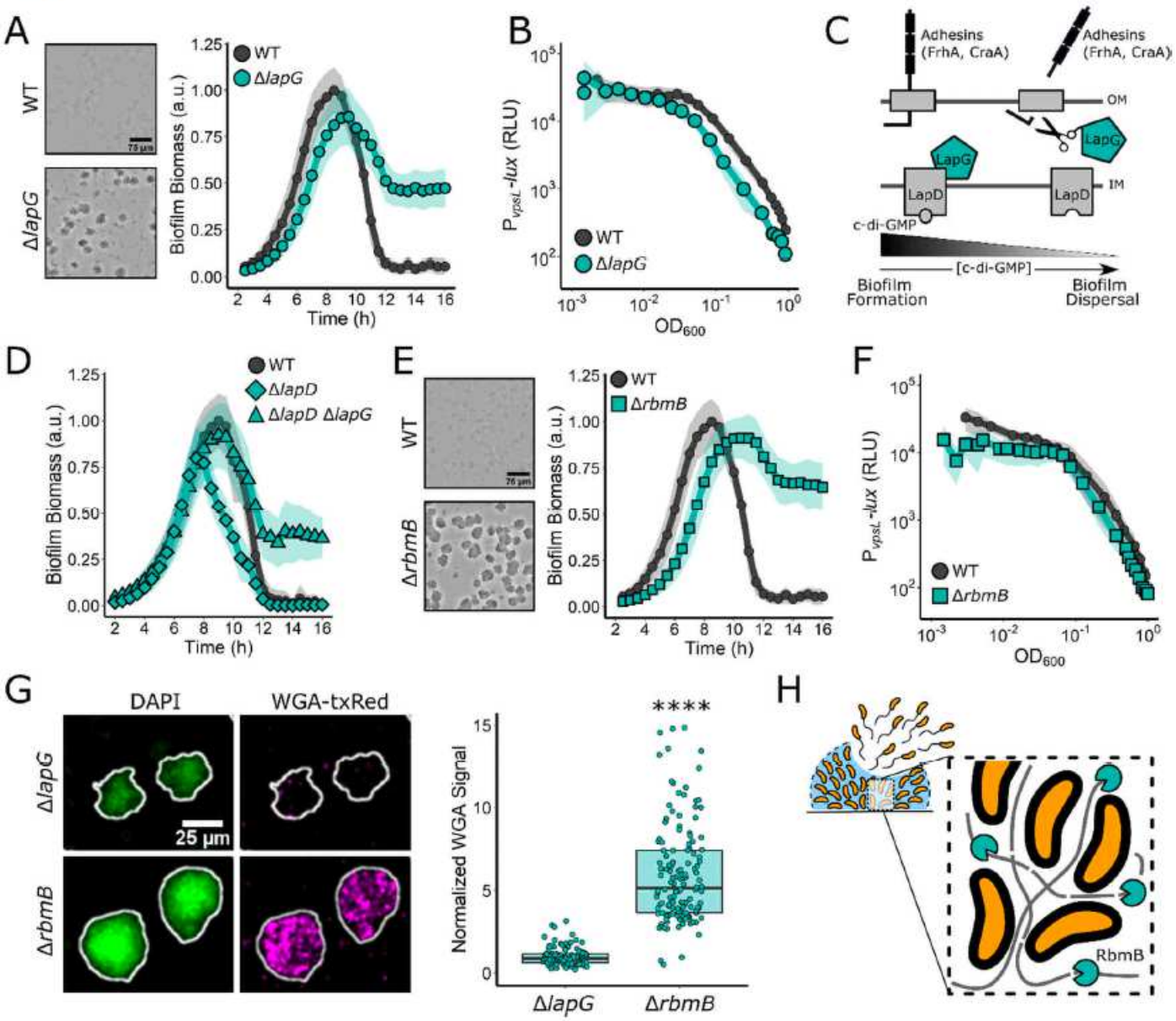

Figure 3

Matrix-digesting enzymes mediate V. cholerae biofilm dispersal. (A) Representative 16 h images and quantitation of biofilm biomass over time measured by time-lapse microscopy for WT V. cholerae and the ΔlapG mutant. (B) The corresponding PvpsL-lux output for strains and growth conditions in A over the growth curve. (C) Schematic representing the LapG mechanism. (D) As in A for the WT, the ΔlapD single mutant, and the ΔlapD ΔlapG double mutant. (E) As in A for the WT and the ΔrbmB mutant. (F) As in B for WT V. cholerae and the ΔrbmB mutant. (G) Representative images and quantitation of WGAtxRed signal in ΔlapG and ΔrbmB biofilms 16 h post-inoculation. To account for differences in biomass, the WGA-txRed signal was divided by the 4', 6-diamidino-2-phenylindole (DAPI) signal in each biofilm. Values were normalized to the mean signal for the ΔlapG strain. >100 individual biofilms were quantified for each strain. An unpaired t-test was performed for statistical analysis, with **** denoting $p < 0.0001$. (H) Proposed model for the role of RbmB in biofilm dispersal. Gray lines represent the polysaccharide matrix. In all cases, N = 3 biological and N = 3 technical replicates, ± SD (shaded). a.u., arbitrary unit. For vpsL-lux measurements, N = 3 biological replicates, ± SD (shaded). RLU, relative light units. OM, outer membrane; IM, inner membrane.

Figure 4

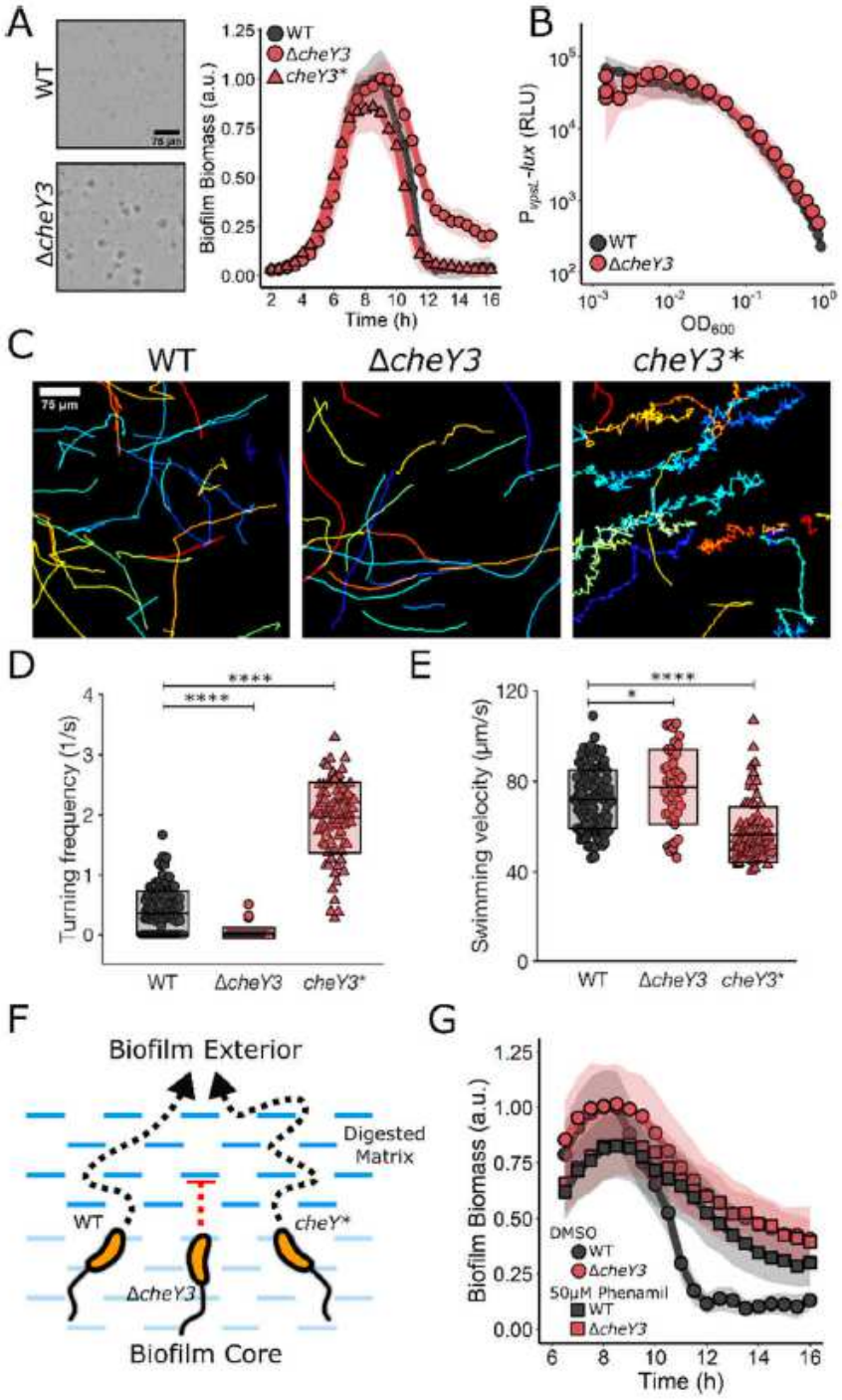

Figure 4

Reorientations in swimming direction are required for V. cholerae biofilm dispersal. (A) Representative 16 h images and quantitation of biofilm biomass over time measured by time-lapse microscopy for WT V. cholerae, the ΔcheY3 mutant, and the cheY3D16K, Y109W (cheY3*) mutant. (B) The corresponding PvpsL-lux output for WT and the ΔcheY3 strain over the growth curve. (C) Representative, randomly colored, single-cell locomotion trajectories for the strains in A. (D) Turning frequencies of the strains in A.

(E) Measured swimming velocities of the strains in A. (F) Proposed model for the role of motility and reorientation in biofilm dispersal. (G) Quantitation of biofilm biomass over time for WT and the ΔcheY3 mutant following treatment with DMSO or the motility inhibitor, phenamil supplied at 5 h post-inoculation. For biofilm biomass assays, N = 3 biological and N = 3 technical replicates, ± SD (shaded). a.u., arbitrary unit. For vpsL-lux measurements, N = 3 biological replicates, ± SD (shaded). RLU, relative light units. For motility measurements, 45-125 individual cells of each strain were tracked. In panels D and E, unpaired ttests were performed for statistical analysis, with P values denoted as *P < 0.05; **P < 0.01; *** P < 0.001; ****P < 0.0001; n.s., P > 0.05.

Supplementary Files

This is a list of supplementary files associated with this preprint. Click to download.

- BridgesSupplementaryVideo1.mov
- SupplementalMaterials.pdf